Identification of the Arabidopsis calmodulin-dependent NAD+ kinase that sustains the elicitor-induced oxidative burst

Elisa Dell'Aglio, Cécile Giustini, Alexandra Kraut, Yohann Couté, Alex Costa, Guillaume Decros, Yves Gibon, Christian Mazars, Michel Matringe, Giovanni Finazzi, et al.

▶ **To cite this version:**

Elisa Dell'Aglio, Cécile Giustini, Alexandra Kraut, Yohann Couté, Alex Costa, et al.. Identification of the Arabidopsis calmodulin-dependent NAD+ kinase that sustains the elicitor-induced oxidative burst. Plant Physiology, 2019, 181 (4), pp.1449-1458. 10.1104/pp.19.00912 . hal-02361156

HAL Id: hal-02361156
https://hal.science/hal-02361156

Submitted on 13 Nov 2019

HAL is a multi-disciplinary open access archive for the deposit and dissemination of scientific research documents, whether they are published or not. The documents may come from teaching and research institutions in France or abroad, or from public or private research centers.

L'archive ouverte pluridisciplinaire **HAL**, est destinée au dépôt et à la diffusion de documents scientifiques de niveau recherche, publiés ou non, émanant des établissements d'enseignement et de recherche français ou étrangers, des laboratoires publics ou privés.

The Arabidopsis Calmodulin-dependent NAD^+ kinase sustaining the elicitor-induced oxidative burst

Elisa Dell'Aglio[a,b], Cécile Giustini[a], Alexandra Kraut[c], Yohann Couté[c], Alex Costa[d], Guillaume Decros[e], Yves Gibon[e,f], Christian Mazars[g], Michel Matringe[a], Giovanni Finazzi[a], Gilles Curien[a]*

[a] Univ. Grenoble Alpes, CNRS, CEA, INRA, BIG-LPCV, 38000 Grenoble, France

[b] Department of Botany and Plant Biology, University of Geneva, 1211 Geneva, Switzerland

[c] Univ. Grenoble Alpes, CEA, INSERM, BIG-EdyP, 38000 Grenoble, France

[d] Department of Biosciences, University of Milan, 20133 Milan, Italy

[e] UMR1332 BFP, INRA, Univ. Bordeaux, Villenave d'Ornon, France

[f] MetaboHUB, Bordeaux, Villenave d'Ornon, France

[g] Laboratoire de Recherche en Sciences Végétales, Université de Toulouse, CNRS, UPS, 24, Chemin de Borde-Rouge, Auzeville, BP 42617, 31326 Castanet-Tolosan, France.

* To whom correspondence may be addressed. E-mail: gilles.curien@cea.fr

Running title: Plant calmodulin-dependent NAD^+ kinase

Abstract

NADP(H) is an essential cofactor of multiple metabolic processes in all living organisms. In plants, NADP(H) is required as the substrate of Ca^{2+}-dependent NADPH oxidases which catalyze a reactive oxygen species burst in response to various stimuli. While $NADP^+$ production in plants has long been known to involve a Calmodulin and Calcium (CaM)/Ca^{2+}- dependent NAD^+ kinase, the nature of the enzyme catalyzing this activity has remained enigmatic, as well as its role in plant physiology. Here, thanks to a combination of proteomics, biochemistry, molecular biology and *in vivo* studies, we have identified an Arabidopsis protein that catalyzes $NADP^+$ production exclusively in the presence of CaM/Ca^{2+}. This new enzyme (NADKc) has a CaM-binding peptide located in its N-terminal region and displays peculiar biochemical properties as well as different domain organization compared to known plant NAD^+ kinases. In response to a pathogen elicitor, activity of NADKc, which is associated with the mitochondrial periphery, contributes to an increase in the cellular $NADP^+$ concentration and to the amplification of the elicitor-induced oxidative burst. Based on a phylogenetic analysis and enzymatic assays, we propose that the CaM/Ca^{2+}-dependent NAD^+ kinase activity found in photosynthetic

organisms is carried out by NADKc-related proteins. Thus, NADKc represents the missing link between Ca^{2+} signalling, metabolism and the oxidative burst.

Keywords: NAD^+ kinase, Calmodulin, Calcium, $NADP^+$, zeta toxin, flagellin22, *Arabidopsis thaliana*.

Introduction

As sessile organisms, plants have evolved mechanisms to react quickly to stress conditions, such as changes in temperature, salinity or pathogen attacks. A common response to stress is a cytosolic calcium (Ca^{2+}) influx followed by an apoplastic burst of Reactive Oxygen Species, or ROS burst (Grant et al., 2000). This ROS burst is generated by plasma membrane NADPH oxidases known as RBOH (for Respiratory Burst Oxidase Homologs, Torres and Dangl, 2005) and in turn regulates adaptation mechanisms such as gene expression, epigenetic changes and long-distance signal transduction (Liebthal and Dietz, 2017; Choi et al., 2017; Chapman et al., 2019). RBOH oxidase activity is dependent on Ca^{2+} binding to their EF-hand domains and is stimulated by phosphorylation by Ca^{2+}-dependent Protein Kinases (Dubiella et al., 2013) as well as CIPK/CBL complexes (Calcineurin B-Like Protein - CBL-Interacting Protein Kinase, Drerup *et al*., 2013).

A rapid increase in the NADP(H) pool size was observed in response to plant treatment with a pathogen elicitor (Harding et al., 1997; Pugin et al., 1997) and may be required to sustain the ROS burst by fuelling RBOH proteins. Since most (~70-90%) of plant NAD^+ kinase activity is dependent on binding Calmodulin (CaM) in its Ca^{2+}-loaded conformation (Anderson and Cormier, 1978) it was proposed (Harding et al., 1997) that the protein responsible for this activity may also be stimulated by the elicitor-induced Ca^{2+} influx. $NADP^+$ produced by this enzyme may then be converted to NADPH (the substrate of RBOH proteins) by NADP-isocitrate dehydrogenase (Mhamdi et al., 2010) or by the reducing branch of the oxidative pentose phosphate pathway (Pugin et al., 1997; Scharte et al., 2009).

Several studies have described the CaM/Ca^{2+}-dependent NAD^+ kinase activity in plants using partially purified enzymatic preparations from plant tissues. These studies allowed to find this protein activity in a wide variety of plant species (Dieter and Marmé, 1984; Delumeau et al., 2000; Turner et al, 2004), and to characterize its kinetic parameters (Delumeau et al., 2000; Turner et al., 2004) as well as its preferences for specific CaM and CaM-like isoforms (Turner et al., 2004). However, the protein responsible for CaM/Ca^{2+}-dependent NAD^+ kinase activity has not been identified. In particular, among the three Arabidopsis NAD^+ kinases identified to date, the plastidial NADK2 was shown to bind CaM *in vitro* in a Ca^{2+}-dependent way (Dell'Aglio et al., 2013a; Turner et al., 2004), but its activity does not

require CaM binding (Turner et al., 2004). Thus, this lack of knowledge of the identity of the plant CaM-dependent NAD^+ kinase has prevented a thorough characterization of its role in plant physiology, and in particular in the production of the stress-induced ROS burst.

Here, we report the characterization of an *A. thaliana* CaM/Ca^{2+}-dependent NAD^+ kinase that displays all the properties of the elusive enzyme. We show that this NAD^+ kinase, which we named NADKc (for NAD kinase-CaM dependent), is associated with mitochondrial periphery and is involved in sustaining the ROS burst induced by the bacterial elicitor flagellin22.

Results and discussion

NADKc is a new CaM/Ca^{2+}-dependent NAD^+ kinase

We obtained an Arabidopsis protein extract enriched in CaM/Ca^{2+}-dependent NAD^+ kinase activity by a four-step purification procedure described in Supplemental Material and Methods. The last step consisted in binding the protein on a CaM-charged matrix in the presence of Ca^{2+} and its subsequent release with an excess of the Ca^{2+} chelator EGTA (Fig. S1). We then used mass spectrometry-based proteomics to identify proteins that were enriched in the EGTA elution compared to the Ca^{2+}-containing washing steps (Supplemental Table S1). We reasoned that putative CaM/Ca^{2+}-dependent NAD^+ kinases should display the following characteristics: *i)* have a molecular weight between 50 and 65 kDa, to respect the size range previously calculated by Delumeau et al., 2000; *ii)* be annotated as ATP-binding proteins (but not as a protein kinase), since it is known that plant CaM-activated NAD kinase uses ATP as a substrate (Anderson and Cormier, 1978); *iii)* contain a predicted CaM-binding site (following the guidelines of Rhoads and Friedberg, 1997) and *iv)* have no previously assigned enzymatic activity. Our analysis revealed only one protein – encoded by the At1g04280 gene – that fulfilled all these criteria.

To confirm its CaM/Ca^{2+}-dependent NAD^+ kinase activity, we expressed the full-length recombinant protein coded by At1g04280 in *E. coli* with an N-terminal His-tag. We compared the NAD^+ kinase activity of two *E. coli* extracts: one obtained from an At1g04280-expressing strain and the second from a strain containing an empty vector. As shown in Fig. 1A, no NAD^+ kinase activity (which in our test was detected as an increase of absorbance at 340 nm) was detected in the *E. coli* strain containing the

empty vector, not even after the addition of an excess of Ca^{2+} and of *A. thaliana* Calmodulin 1 (AtCaM1). In contrast, addition of the At1g04280-expressing *E. coli* extract to the same reaction mixture immediately revealed NAD^+ kinase activity.

Activity measurements with a partially purified At1g04280 enzyme confirmed the lack of NAD^+ kinase activity in the absence of AtCaM1/Ca^{2+} and its appearance, within seconds, upon addition of both AtCaM1 and Ca^{2+}. This NAD^+ kinase activity was suppressed by EGTA and restored by the addition of an excess of Ca^{2+}, showing that the CaM/Ca^{2+}-dependent enzyme activation is an all-or-none, reversible process (Fig. 1B). In contrast, while a CaM/Ca^{2+}-dependent NAD^+ kinases have also been described in invertebrates, animal NAD^+ kinase activity is only slightly increased by CaM/Ca^{2+} addition. For example, CaM induces a 3.5-fold increase of the NADK-2 activity of the sea urchin *Strongylocentrotus purpuratus* (Love et al., 2015).

Based on these results, we identified the At1g04280 gene product as the long-sought CaM/Ca^{2+}-dependent NAD^+ kinase enzyme previously found in several plant species (Anderson and Cormier, 1978, Delumeau et al., 1998, Turner et al., 2004) and named it *A. thaliana* "NADKc" for "NAD kinase-CaM dependent".

AtNADKc peculiar features in primary sequence and enzyme activity

The primary sequence of NADKc (Fig. 1C) contains: *i)* an N-terminal region predicted to contain a transmembrane helix (amino acids: 1-45); *ii)* a domain of unknown function (amino acids 46-225) that includes a conserved putative CaM-Binding Site (CBS, Fig S2A); and *iii)* a C-terminal kinase domain (amino acids 226-340) similar to bacterial type II zeta-toxin domains (Khoo et al., 2007), which is predicted to contain a conserved P-loop for ATP binding (Walker A motif, WM, amino acids: 236-250, Fig S2B). Interestingly, these features are not shared with all other NAD^+ kinases known to date, from bacteria, plants and animals (Fig. 1C, Kawai et al, 2001; Turner et al., 2004, Chai et al., 2006; Love et al., 2015).

To optimize NADKc expression levels in *E. coli* and improve the solubility of the protein, we removed the first 38 residues constituting the predicted transmembrane helix. The shorter version, 6HIS-

Δ38NADKc was partially purified by Ni-NTA affinity chromatography (Fig. S3, lane 3). Activity assays with saturating AtCaM1/Ca^{2+} concentrations revealed the NAD^+ kinase activity of NADKc to be specific toward NAD^+, as no activity could be detected with NADH or deamido-NAD^+ (NAAD) (Table 1). Like most P-loop-containing kinases (Das et al., 2013), the enzyme displayed broad specificity for the phosphoryl donor, as ATP, CTP, GTP and UTP could be used indifferently and produced similar efficiencies (Table 1). The enzyme catalytic constant with CTP or ATP was close to 40 s^{-1} in the presence of Ca^{2+} and AtCaM1, *i.e.* about 10-fold higher than that reported for plant CaM/Ca^{2+}-independent NAD^+ kinases and other NAD^+ kinases from bacteria and animals (0.5-7 s^{-1}, (Kawai et al., 2001; Chai et al., 2006; Love et al., 2015; Turner et al., 2004)).

To characterize the interaction of NADKc with CaM, we further purified the recombinant enzyme by urea denaturation and rapid dilution (see Supplemental Material & Methods). The refolded protein (Fig S3, lanes 4-5) produced a single band on an SDS-PAGE gel and had an increased catalytic constant (70 s^{-1}) compared to the partially purified enzyme (40 s^{-1}, Table 1) and high affinity for CaM (k_d = 0.6-1 nM, Fig. 1D), similar to the value of 0.4 nM reported for the tomato CaM-dependent NAD^+ kinase (Delumeau et al., 2000).

In conclusion, compared to all other NAD^+ kinases known to date, NADKc displays unique structural as well as catalytic features which make it particularly suitable for rapid $NADP^+$ production following Ca^{2+} signals.

Identification of a CaM-binding peptide in the NADKc N-terminal domain

To verify that the NADKc N-terminal domain is involved in CaM-binding, we measured NADKc activity in the presence of a synthetic peptide containing the putative "type A 1-8-14" CaM-binding sequence (amino acids 167-196, Fig. 1C, Rhoads and Friedberg, 1997) in a competitive assay. As shown in Fig. 1E, the presence of the putative NADKc CaM-binding peptide decreased the stimulation of NADKc by AtCaM1, as expected if AtCaM1, trapped by the peptide in excess, was no longer available for NADKc activation. The reduction in reaction rate was hyperbolically related to the peptide concentration (IC50 =0.5 μM). In contrast, another unrelated peptide from the Tic32 protein, which

cannot specifically bind AtCaM1 (Dell'Aglio, 2013b), was also tested. An excess of this control peptide had no effect on NAD^+ kinase activity (Fig. 1E).

These data suggest that the NADKc peptide identified plays a major role in the AtCaM1/Ca^{2+}-dependent activation of the NADKc enzyme. We hypothesize that it could be an anchoring point for CaM in the full-length protein, facilitating activation of the kinase domain by an as yet unknown mechanism.

NADKc is located at the mitochondrial periphery

To assess the NADKc localization *in vivo*, we produced strains containing several YFP-tagged NADKc versions: *i.)* the NADKc full-length protein fused to YFP at its C-terminal (construct NADKc-YFP); *ii.)* the NADKc N-terminal region (amino acids 1-45) fused to YFP (construct $NADKc_{Nter}$-YFP); the YFP fused at the N-terminus of the whole NADKc protein sequence (construct YFP-NADKc). All fusion proteins were inserted into expression plasmids under the control of the CaMV 35S promoter.

Arabidopsis lines and tobacco leaves containing the NADKc:YFP construct showed protein clusters that likely constitute non-specific aggregates caused by high expression of a membrane construct (not shown). However, in tobacco leaves (see Fig. S4, upper and middle row) and Arabidopsis seedlings, the $NADKc_{Nter}$-YFP was targeted to ring-like structures in both stomata (Fig. 2 A-F) and root tip cells. In the root tips, the $NADKc_{Nter}$-YFP protein co-localized with the mitochondrial matrix marker Tetramethylrhodamine, methyl ester (TMRM), but the fluorescence signal of $NADKc_{Nter}$-YFP was more peripheral than the TMRM signal (Fig. 2, G-I). As a comparison, we observed Arabidopsis root tip cells expressing NMT1-GFP, an outer mitochondrial membrane protein (Fig. 2, J-L, Wagner et al., 2015), as well as MT-cp-YFP (Fig. 2, M-O), a pH biosensor located in the mitochondrial matrix (Schwarzländer et al., 2011; Behera et al., 2018). This comparison clearly showed a higher resemblance of the $NADKc_{Nter}$-YFP signal profile to the NMT1-GFP profile than to the MTcp-YFP profile, suggesting a localization at the outer mitochondrial membrane.

To corroborate this conclusion we measured the pixel intensity distribution of various TMRM-stained mitochondria from $NADKc_{Nter}$-YFP transformed plants. While the TMRM fluorescence intensity peak was located at the centre of the mitochondria, $NADKc_{Nter}$-YFP fluorescence intensity formed two

distinctive peaks at opposite sides from the centre where fluorescence intensity was at its minimum (Fig. 2, P-R). This pattern matches the one previously measured for the outer-membrane localized NMT1-GFP protein (Wagner et al, 2015).

We successfully achieved expression of YFP-NADKc only in transiently transformed tobacco leaves, where fluorescence was dispersed inside the cytosol (Fig. S4, bottom line). This result was probably due to the NADKc N-terminus being hidden in the middle of the sequence and is consistent with the hypothesis that the N-terminal region of NADKc is important for the protein to be correctly addressed to the mitochondria.

Protein overexpression by a strong promoter as CaMV 35S is prone to promote protein aggregates and overexpression artefacts. However, using cell fractionation, early works on the CaM/Ca^{2+}-dependent NAD^+ kinase activity in plants located this enzyme at the mitochondrial periphery (either inner or outer mitochondrial membrane) in both maize (Dieter and Marmé, 1984; Sauer and Robinson, 1985) and *Avena sativa* (Pou de Crescenzo et al., 2001). More recently, NADKc was detected in the mitochondria by two proteomic studies (Klodmann et al., 2011, Wagner et al., 2015) and at the plasma membrane by one study (Mitra et al., 2009). Our results therefore corroborate and extend previous findings obtained using different approaches.

NADKc enhances Flg22 response in Arabidopsis seedlings

To investigate the physiological role of NADKc, we analysed the two Arabidopsis T-DNA insertion lines SALK_006202 and GABI-KAT 311H11, hereafter called *nadkc-1* and *nadkc-2* (Fig. 3A). NADKc transcripts were reduced by more than 95% in both lines (Fig. 3B).

To confirm the unique role of NADKc for CaM/Ca^{2+}-dependent $NADP^+$ production in Arabidopsis seedlings, NAD^+ kinase activity was measured in protein extracts from Col-0 and mutant seedlings, both in the presence of trifluoroperazine (TFP) - a CaM inhibitor - and AtCaM1/Ca^{2+} (Fig. 3C). In Col-0 plants, the activity measured in the presence of AtCaM1/Ca^{2+} was more than 10-fold higher than in the presence of TFP, while in *nadkc-1/2* mutants, no difference was observed between the two conditions. In both mutants, activity levels were close to those measured in Col-0 plants in the presence of TFP,

confirming the absence of NADKc activity in these mutants. Consistent with these results, two complemented lines obtained by stably transforming *nadkc-1* with full-length NADKc under the control of the CaMV 35S promoter (lines *nadkc-1*_NADKc-1 and *nadkc-1*_NADKc-2) - had NADKc activity levels similar to Col-0 (Fig. 4D).

Neither *nadkc* mutant showed any visible growth impairment when grown under short day or long day photoperiods (Fig. S5, A-B) and photosynthetic parameters (Fv/Fm, ETR and NPQ, (Maxwell and Johnson, 2000)) were the same in all genotypes (Fig. S5, C-E). This suggests that NADKc is not involved in photosynthesis-driven growth.

As CaM-dependent NAD^+ kinase activity was previously associated with the generation of the oxidative burst triggered by plant response to elicitors (Grant et al., 2000; Harding et al., 1997), we expected to observe a decrease in a pathogen elicitor-induced extracellular ROS burst in *nadkc-1/2* mutants coupled with lower NADP pools with respect to Col-0 seedlings.

We therefore exposed 7-day-old Arabidopsis seedlings to the bacterial elicitor flg22, followed by measurements of $NAD(P)^+$ and NAD(P)H concentrations and ROS production. As shown in Fig. 3E, no statistically significant differences were observed between Col-0 and *nadkc-1* in $NAD(P)^+$ and NAD(P)H concentrations before the flg22 treatment. However, the flg22 challenge induced an increase in the Col-0 $NADP^+$ cellular concentration, which was absent in the *nadkc* seedlings. Moreover, dramatic reduction in ROS accumulation (more than 90%) was observed in the *nadkc-1/2* mutants (Fig. 3F), but complementation with the NADKc full-length protein restored ROS accumulation up to wild-type levels (Fig. 3G).

Based on these results, we propose a role for NADKc in producing NADP(H) needed to sustain the elicitor-induced ROS burst in Arabidopsis seedlings (Fig. 4).

Distribution of CaM-dependent NAD^+ kinase activity in the green lineage

The domain organization of NADKc (*i.e.*, a ca 200 amino acid domain of unknown function at the N-terminus with a putative CBS followed by a kinase domain annotated “zeta toxin domain”, Fig. 1C) was only found in higher plants and some algae.

To better trace the evolution of the plant CaM-dependent NAD^+ kinase, we compared gene sequences and NADK activity in several plants and algae and we built a maximum likelihood phylogenetic tree with representative putative NADKc proteins (Fig. S6). The phylogenetic tree showed that plant NADKc-like proteins form four major clusters that correspond to the main plant phylogenetic groups with the exception of Gymnosperms and Pteridophytes. Many plants, especially dicots, contain several genes encoding for this protein, suggesting duplication events across evolution. Interestingly, the two other NADKc homologues present in the Arabidopsis genome (At1g06750 and At2g30630) seem to have a pollen-specific expression pattern (Krishnakumar et al., 2014).

Among algae, while the genomes of *Chlamydomonas reinhardtii*, *Ostreococcus taurii* and *Chara braunii* appeared devoid of NADKc-like sequences, the genomes of *Coccomyxa subellipsoidea*, *Ulva mutabilis*, *Klebsormidium flaccidum*, *Spyrotaenia minuta*, *Entransia fimbriata*, Mougeotia sp. and Spirogyra sp. all harbour one NADKc-like sequence. In particular, NAD^+ kinase genes of *Klebsormidium flaccidum*, *Entransia fimbriata*, Mougeotia sp. and Spirogyra sp. contain a clear CBS, while in *Coccomyxa subellipsoidea*, *Ulva mutabilis* and *Spirotaenia minuta*, this region is less conserved (Fig. S2A). In agreement with the genomic survey, CaM-dependent NAD^+ kinase activity could be successfully measured in the moss *M. polymorpha* and filamentous alga *K. flaccidum*, but not in the unicellular alga *C. reinhardtii* (Table 2).

Interestingly, both the total CaM-dependent NAD^+ kinase activity and the percentage of CaM-dependent NADK-activity on the total NADK activity increase from *K. flaccidum* (4.0 $nmol \cdot h^{-1} \cdot mg^{-1}$; 66.7%) to *M. polymorpha* (5.9 $nmol \cdot h^{-1} \cdot mg^{-1}$; 85.7%) and to *A. thaliana* (30.2 $nmol \cdot h^{-1} \cdot mg^{-1}$; 96.8%). It is therefore possible that the importance of the CaM control on NADKc-like proteins increased during the evolution of plant lineage and became a key element of the ROS response to elicitors in angiosperms, and quite likely other abiotic/biotic stress conditions that trigger Ca^{2+} fluxes.

Conclusions

Overall, we have identified unambiguously NADKc as the CaM/Ca^{2+}-dependent NAD^+ kinase of Arabidopsis seedlings. Its identification allows answering earlier questions concerning its physiological

role: consistent with its localization at the mitochondrial periphery, this enzyme has no role in photosynthesis, but can regulate the ROS burst by sustaining the activity of RBOH proteins. Besides being essential for the elicitor-induced oxidative burst of Arabidopsis, this enzyme may participate in other plant developmental and stress responses involving Ca^{2+} fluxes. This would stem from the evolutionary recruitment of a distinctive combination of a CaM-binding region and a type II zeta-toxin domain, which would provide it with regulatory properties different from its animal counterpart.

Material and Methods

Chemicals

All chemicals were from Sigma Aldrich.

Plant growth and isolation of homozygous NADKc lines

A. thaliana Col-0 ecotype was used in this study. Plants were grown under 65% humidity and either long day (16 h light – 85 µmol photons·m^{-2}·s^{-1}, 8 h dark) or short day (8 h light – 90 µmol photons·m^{-2}·s^{-1}, 16 h dark) conditions. Day-time temperature was set to 20 °C, and night-time temperature to 18 °C.

The two T-DNA insertion lines, *nadkc-1* (SALK_006202) and *nadkc-2* (GABI_311H11), were obtained from NASC/ABRC (Alonso et al., 2003; Kleinboelting et al., 2012). Lines were selected in the appropriate antibiotic (kanamycin for *nadkc-1* and sulfadiazine for *nadkc-2*) and genotyped by PCR using left border primers LBb1.3 (*nadkc-1*) or LB GABI-KAT (*nadkc-2*) and the appropriate specific primers listed in Supplemental Table S2. PCR products were sequenced to confirm the precise position of each insertion.

Klebsormidium flaccidum (Hori et al., 2014) (SAG335-2b curated as *Klebsormidium nitens*) was obtained from EPSAG (Department of Experimental Phycology and Culture Collection of Algae, Göttingen Universität, Germany). The alga was grown on agar plates under continuous light (60 µmol

photons·m^{-2}·s^{-1}) in the Modified Bolds 3N Medium (https://utex.org/products/modified-bolds-3n medium) without vitamins.

M. polymorpha was collected in the forest (GPS coordinate: 45.335088 , 5.632257) and *Chlamydomonas reinhardtii* (C137 strain) was grown in TAP medium at 24°C under continuous low white light (40 µmol photons·m^{-2}·s^{-1}) exposure. Protein extracts were prepared as described in the supplementary information for Arabidopsis.

Additional Material and Methods procedures are described in the Supplementary Information.

Author contributions

E.D., C.M., G.F. and G.C. designed the experiments and analyzed the data; E.D., C.G., M.M., A.K., Y.C., A.C. G.F., C.M., G.D., Y.G. and G.C. conducted the experiments. E.D., G.F., C.M. and G.C. wrote the article with contributions from all the authors. G.C. agrees to serve as the author responsible for contact and ensures communication.

Accession numbers

Sequence data from this article can be found in the EMBL/GenBank data libraries under accession number: At1g04280; UniProt accession: Q0WUY1.

Acknowledgments

This work was supported by the French National Research Agency (grant no. ANR-10-13 LABEX-04 GRAL Labex, Grenoble Alliance for Integrated Structural Cell Biology). G.F. acknowledges support from the HFSP grant RGP0052/2015 (photosynthetic light utilization and ion fluxes: making the link) and A.C. to UNIMI PIANO DI SVILUPPO DI ATENEO, Transition Grant 2015/2017 – Horizon 2020 Linea 1A. The proteomic analyses were partially supported by the French National Research Agency ProFI Grant (ANR-16 10-INBS-08-01). Part of this work was carried out at NOLIMITS, an advanced imaging facility established by the University of Milan.

We are grateful to Markus Schwarzländer (University of Münster, Germany) for providing the NMT1:GFP and MT-cp:YFP Arabidopsis lines. We thank Elsa Clavel-Coibrié for help with analysis of the complemented mutant plants.

References

Alonso JM, Stepanova AN, Leisse TJ, Kim CJ, Chen H, Shinn P, Stevenson DK, Zimmerman J, Barajas P, Cheuk R, et al (2003) Genome-wide insertional mutagenesis of *Arabidopsis thaliana*. Science **301:** 653-657

Anderson JM, Cormier MJ (1978) Calcium-dependent regulation of NAD kinase. Biochem Biophys Res Commun **84:** 595-602

Behera S, Zhaolong X, Luoni L, Bonza MC, Doccula FG, De Michelis MI, Morris RJ, Schwarzländer M, Costa A (2018) Cellular Ca^{2+} signals generate defined pH signatures in plants. Plant Cell **30:** 2704-2719

Chai MF, Wei PC, Chen QJ, An R, Chen J, Yang S, Wang XC (2006) NADK3, a novel cytoplasmic source of NADPH, is required under conditions of oxidative stress and modulates abscisic acid responses in Arabidopsis. Plant J **47:** 665-674

Chapman JM, Muhlemann JK, Gayomba SR, Muday GK (2019) RBOH-Dependent ROS Synthesis and ROS scavenging by plant specialized metabolites to modulate plant development and stress responses. Chem Res Toxicol. **32:** 370-396

Choi WG, Miller G, Wallace I, Harper J, Mittler R, Gilroy S (2017) Orchestrating rapid long-distance signaling in plants with Ca^{2+}, ROS and electrical signals. Plant J **90:** 698-707

Dell'Aglio E, Giustini C, Salvi D, Brugiere S, Delpierre F, Moyet L, Baudet M, Seigneurin-Berny D, Matringe M, Ferro M, et al (2013a) Complementary biochemical approaches applied to the identification of plastidial calmodulin-binding proteins. Mol Biosyst **9:** 1234-1248

Dell'Aglio E (2013b) The regulation of plastidial proteins by calmodulins: Université de Grenoble.

Delumeau O, Renard M, Montrichard F (2000b) Characterization and possible redox regulation of the purified calmodulin-dependent NAD^+ kinase from *Lycopersicon pimpinellifolium*. Plant Cell Environ **23:** 1267-1273

Dieter P, Marme D (1984) A Ca^{2+}, Calmodulin-dependent NAD kinase from corn is located in the outer mitochondrial membrane. J Biol Chem **259:** 184-189

Drerup MM, Schlücking K, Hashimoto K, Manishankar P, Steinhorst L, Kuchitsu K, Kudla J. (2013) The Calcineurin B-like calcium sensors CBL1 and CBL9 together with their interacting protein kinase CIPK26 regulate the Arabidopsis NADPH oxidase RBOHF. Mol Plant. **6:** 559-69

Dubiella U, Seybold H, Durian G, Komander E, Lassig R, Witte CP, Schulze WX, Romeis T (2013) Calcium-dependent protein kinase/NADPH oxidase activation circuit is required for rapid defense signal propagation. Proc Natl Acad Sci USA. **110:** 8744-9

Grant M, Brown I, Adams S, Knight M, Ainsli A, Mansfield J (2000) The RPM1 plant disease resistance gene facilitates a rapid and sustained increase in cytosolic calcium that is necessary for the oxidative burst and hypersensitive cell death. Plant J **23:** 441-450

Harding SA, Oh SH, Roberts DM (1997) Transgenic tobacco expressing a foreign calmodulin gene shows an enhanced production of active oxygen species. Embo J **16:** 1137-1144

Kawai S, Mori S, Mukai T, Hashimoto W, Murata K (2001) Molecular characterization of Escherichia coli NAD kinase. Eur J Biochem **268:** 4359-65

Khoo SK, Loll B, Chan WT, Shoeman RL, Ngoo L, Yeo CC, Meinhart A (2007) Molecular and structural characterization of the PezAT chromosomal toxin-antitoxin system of the human pathogen *Streptococcus pneumoniae*. J Biol Chem **282:** 19606-19618

Kleinboelting N, Huep G, Kloetgen A, Viehoever P, Weisshaar B (2012) GABI-Kat SimpleSearch: new features of the *Arabidopsis thaliana* T-DNA mutant database. Nucleic Acids Res **40:** D1211-1215

Klodmann J, Senkler M, Rode C, Braun H-P (2011) Defining the protein complex proteome of plant mitochondria. Plant Phys **157:** 587–598

Krishnakumar V, Hanlon MR, Contrino S, Ferlanti ES, Karamycheva S, Kim M, Rosen BD, Cheng C-Y, Moreira W, Mock SA, Stubbs J, Sullivan JM, Krampis K, Miller JR, Micklem G, Vaughn M, Town CD (2015) Araport: the Arabidopsis information portal. Nucleic Acids Research **43:** D1003–D1009

Love NR, Pollak N, Dolle C, Niere M, Chen Y, Oliveri P, Amaya E, Patel S, Ziegler M (2015) NAD kinase controls animal NADP biosynthesis and is modulated via evolutionarily divergent calmodulin-dependent mechanisms. Proc Natl Acad Sci USA **112:** 1386-1391

Liebthal M, Dietz KJ (2017) The fundamental role of reactive oxygen species in plant stress response. Plant Stress Tolerance In: Sunkar R. (eds) Plant Stress Tolerance. Methods in Molecular Biology, **1631:** 23-39. Humana Press, New York, NY.

Maxwell K, Johnson GN (2000) Chlorophyll fluorescence-a practical guide. J Exp Bot **51:** 659-668.

Mhamdi A, Mauve C, Gouia H, Saindrenan P, Hodges M, Noctor G (2010) Cytosolic NADP-dependent isocitrate dehydrogenase contributes to redox homeostasis and the regulation of pathogen responses in Arabidopsis leaves. Plant Cell Env **33:** 1112-1123

Mitra SK, Gantt JA, Ruby JF, Clouse SD, Goshe MB (2007) Membrane proteomic analysis of *Arabidopsis thaliana* using alternative solubilization techniques. J. Proteome Res. **6:** 1933-1950

Pou de Crescenzo M-A, Gallais S, Léon A, Laval-Martin DL (2001) Tween-20 activates and solubilizes the mitochondrial membrane-bound, calmodulin dependent NAD^+ kinase of *Avena sativa* L. J Membr Biol **182:** 135–146

Pugin A, Frachisse JM, Tavernier E, Bligny R, Gout E, Douce R, Guern J (1997) Early events induced by the elicitor cryptogein in tobacco cells: involvement of a plasma membrane NADPH oxidase and activation of glycolysis and the pentose phosphate pathway. Plant Cell **9:** 2077-2091

Rhoads AR, Friedberg F (1997) Sequence motifs for calmodulin recognition. The FASEB Journal **11:** 331–340

Sauer A, Robinson DG (1985) Calmodulin dependent NAD-kinase is associated with both the outer and inner mitochondrial membranes in maize roots. Planta **166:** 227-233

Scharte J, Schön H, Tjaden Z, Weis E, von Schaewen A (2009) Isoenzyme replacement of glucose-6-phosphate dehydrogenase in the cytosol improves stress tolerance in plants. Proc Natl Acad Sci U S A **106:** 8061-8066

Schwarzländer M, Logan DC, Fricker MD, Sweetlove LJ (2011) The circularly permuted yellow fluorescent protein cpYFP that has been used as a superoxide probe is highly responsive to pH but not superoxide in mitochondria: implications for the existence of superoxide 'flashes'. Biochem J. **437:** 381-7

Torres MA, Dangl JL (2005) Functions of the respiratory burst oxidase in biotic interactions, abiotic stress and development. Curr Opin Plant Biol **8:** 397-403

Turner WL, Waller JC, Vanderbeld B, Snedden WA (2004). Cloning and characterization of two NAD kinases from Arabidopsis. Identification of a calmodulin binding isoform. Plant Physiol **135:** 1243-1255

Wagner S, Behera S, De Bortoli S, Logan DC, Fuchs P, Carraretto L, Teardo E, Cendron L, Nietzel T, Füßl M, Doccula FG, Navazio L, Fricker MD, Van Aken O, Finkemeier I, Meyer AJ, Szabò I, Costa A, Schwarzländer M (2015) The EF-hand Ca^{2+} binding protein MICU choreographs mitochondrial Ca^{2+} dynamics in Arabidopsis. The Plant Cell **27:** 3190–3212

Figures legends

Figure 1. Biochemical properties of a CaM-dependent NAD^+ kinase identified in Arabidopsis. (A) NAD^+ kinase activity measured in an *E. coli* extract expressing an empty pET28b(+) and an *E. coli* extract expressing At1g04280. Spikes correspond to the moments of addition of glucose 6-phosphate dehydrogenase (G6PDH), Ca^{2+}, AtCaM1, and *E. coli* extracts (10 μg). (B) NAD^+ kinase activity in an *E. coli* bacterial extract expressing At1g04280. Ca^{2+}, AtCaM1 and EGTA were added at different times, as indicated in the graph. (C) Schematic representation of the NADKc primary sequence and comparison with previously known NAD^+ kinases. Yellow: zeta-toxin domain (InterPro Homologous superfamily: IPR010488); black: N-terminal region with putative organelle target sequence; red: putative conserved Type A 1-8-14 CaM-binding site (detailed below the scheme); orange: Walker A motif (ATP-binding site); blue: NAD^+ kinase domain (InterPro Homologous Superfamily: IPR016064); red/grey: N-terminal sequence expected to contain a CaM-binding site according to Love et al, 2015. Sequences used for comparison (UniProt): *E. coli* NAD^+ kinase: P0A7B3; *A. thaliana* NAD^+ kinases: AtNADK1: Q56YN3; AtNADK2: Q9C5W3; AtNADK3: Q500Y9; *Strongylocentrotus purpuratus* NAD^+ kinase-2 (sea urchin CaM-dependent NAD^+ kinase, Love et al., 2015): C3RSF7. (D) Affinity of NADKc recombinant protein for AtCaM1: Activity of the purified NADKc recombinant protein after denaturation in urea and subsequent refolding was measured in the presence of 50 μM Ca^{2+} and as a function of [AtCaM1]. Experiments were performed in triplicate and data shown are from one representative experiment.

Binding data were analysed assuming tight binding. K_d value for AtCaM1 binding varied from 0.6 to 1 nM. (E) Inhibition of NADKc activity by competition with the putative CaM-binding site (black dots). Black squares correspond to results obtained with a negative control peptide, which does not bind AtCaM1.

Figure 2. Analysis of submitochondrial localization of $NADKc_{Nter}$-YFP. (A to C) Confocal laser scanning microscopy images from stomata guard cells of a representative Arabidopsis seedling stably expressing $NADKc_{Nter}$-YFP. Scale bar = 5 µm. (D to E) Higher magnification of the region of interest shown in A to C (white squares). Scale bar = 1 µm. (A, D) YFP fluorescence in green; (B, E) chlorophyll fluorescence in blue; (C, F) merge between YFP and chlorophyll fluorescences. (G to I) Confocal laser scanning microscopy images from root tip cells of a representative Arabidopsis seedling stably expressing $NADKc_{Nter}$-YFP and stained with the mitochondrial matrix marker TMRM. Scale bar = 1 µm. (J to L) Confocal laser scanning microscopy images from root tip cells of a representative Arabidopsis seedling stably expressing NMT-GFP and stained with the mitochondrial matrix marker TMRM. Scale bar = 1 µm. (M to O) Confocal laser scanning microscopy images from root tip cells of a representative Arabidopsis seedling stably expressing MT-cpYFP and stained with the mitochondrial matrix marker TMRM. Scale bar = 1 µm. (G, M) YFP fluorescence in green; (J) GFP fluorescence in green; (H, K and N) TMRM fluorescence in magenta; (I, L and O) merge between YFP/GFP and TMRM fluorescences. NMT1-GFP and MT-cpYFP were used as markers for the mitochondrial outer mitochondrial membrane (OMM) and matrix, respectively. (P to R) Normalized pixel intensity distributions in the YFP and TMRM fluorescence channels plotted centrally across three individual mitochondria of a seedling expressing the $NADKc_{Nter}$-YFP.

Figure 3. The CaM/Ca^{2+}-dependent NAD^+ kinase activity of Arabidopsis seedlings is absent in *nadkc* mutants. (A) schematic representation of the NADKc gene and position of the T-DNA insertions in the *nadkc-1* and *nadkc-2* mutant lines. (B) NADKc transcript levels in Col-0 and *nadkc*-mutant seedlings. Levels are expressed relative to GAPDH. Data shown correspond to mean +/- s.d., n=3. (C) NAD^+ kinase activity measured in Col-0 and *nadkc* mutant plants (7-day-old whole plantlets), in the presence of the CaM inhibitor TFP (40 µM) or AtCaM1 (250 nM) and Ca^{2+} (0.5 mM). Values correspond to the average of four replicates. (D) NAD^+ kinase activity measured in Col-0 and mutant plants complemented

with NADKc gene (*nadkc-1*_NADKc-1 and *nadkc-1*_NADKc-2) in 7-day-old whole plantlets, in the presence of the CaM inhibitor TFP (40 μM) or of AtCaM1 (250 nM) and Ca^{2+} (0.5 mM). (E) $NAD(P)^+$ and NAD(P)H concentrations in 7-day-old seedlings exposed (flg22, 1 μM) or unexposed (H_2O) for 12 min. to the bacterial elicitor flagellin22. (80-100 mg of tissue per measure, data shown correspond to mean +/- s.e.m. for 3 biological replicates). (F) Flg22 (1 μM)-induced oxidative burst in 7-day-old Col-0 and *nadkc* mutant seedlings (30 plantlets per well, data shown correspond to mean +/- s.d. for 4 wells). (G) Flg22 (1 μM)-induced oxidative burst in Col-0, *nadkc-1* mutant and mutant plants complemented with NADKc gene (*nadkc-1*_NADKc-1 and *nadkc-1*_NADKc-2); 7-day-old seedlings, 30 plantlets per well. Data shown correspond to mean +/- s.d. for 4 wells. Asterisks indicate a significant difference between two conditions based on a Welch's t test (*$p < 0.05$; ***$p < 0.001$).

Figure 4. Hypothetical model of the role of CaM/Ca^{2+}-dependent NADKc in sustaining the flg22-induced oxidative burst in Arabidopsis seedlings. Numbers refer to known sequential events; red numbers highlight events related to NADKc activation: 1. binding of Flg22 elicitor to the Fls2 receptor (Sun et al., 2013); 2. activation of proton efflux and Ca^{2+} influx; 3a. Ca^{2+}-dependent activation of CDPKs and CIPK/CBLs that phosphorylate RBOH proteins; 3b. Ca^{2+} binding to RBOH proteins; 3c. Ca^{2+} binding to CaM, leading to CaM structural modification and formation of the CaM/NADKc complex; 4. activation of $NADP^+$ production by NADKc; 5. increased flux in the oxidative pentose phosphate pathway (OPPP), leading to a higher availability of NADPH; 6. production of the extracellular oxidative burst by NADPH oxidases (RBOH proteins).

Table 1. NADKc kinetic parameters.

Table 2. Comparison of CaM-dependent NADK activity in different photosynthetic organisms. NADK activity ($nmol \cdot h^{-1} \cdot mg^{-1}$ protein) was measured in soluble protein extracts from *Arabidopsis thaliana*, *Marchantia polymorpha*, *Klebsormidium flaccidum* and *Chlamydomonas reinhardtii* as detailed in Methods. Activities are expressed in nmol/h/mg protein. [a]NADK activity measured in the presence of CaM/Ca^{2+} represents CaM-independent plus CaM–dependent activity; [b]NADK activity measured in the presence of trifluoroperazine (CaM inhibitor) represents CaM-independent NADK activity. [c]CaM/Ca^{2+}-dependent activity is the difference between total NADK activity and CaM/Ca^{2+}-independent activity.

NADK activity in C. *reinhardtii* is independent on CaM/Ca^{2+} (the difference is within experimental error).

Supplemental Material and Methods

Partial purification of native NADKc

To purify native CaM-dependent NAD^+ kinase, Col-0 Arabidopsis plants seeds were sterilized, sown in Murashige and Skoog (Murashige and Skoog, 1962) liquid medium (2.2 g L^{-1}) supplemented with 0.5 g L^{-1} sucrose and grown under continuous light (60 µE) in 250-mL flasks and under agitation (125 rpm). Seven-day-old plants were rinsed with water, frozen in liquid nitrogen and ground with a mortar and pestle. The powder was suspended in Buffer A (50 mM Tris-HCl pH 7.5, 400 mM KCl, 3 mM $MgCl_2$, 1 mM EGTA, 0.5 mM EDTA, 1 mM DTT, 1 mM NAD^+, 10 µM leupeptine, 10 µM E64, 1 mM PMSF, 1 mM benzamidine and 5 mM ε-aminocaproic acid). The crude extract was centrifuged (15,000 g, 30 min, 4 °C) and the recovered soluble protein extract (432 mg, 72 mL, 0.74 µmol h^{-1} mg^{-1}) was precipitated with 50% ammonium sulfate (1 h, 4 °C) and centrifuged (20,000 *g*, 20 min). The protein pellet was then suspended in 32 mL Buffer A (30 mL, 270 mg, 1.1 µmol h^{-1} mg^{-1}) and loaded onto a DEAE column (60 mL resin) equilibrated with Buffer A. AtCaM1/Ca^{2+}-dependent NADK activity was detected in the flow-through (120 mL, 84 mg, 1.8 µmol h^{-1} mg^{-1}). NaCl (3.5 M) was added to this fraction, and the protein solution was loaded onto a Butyl-Sepharose column (12 mL resin) equilibrated with Buffer B - NaCl (50 mM Tris-HCl pH 7.0, 3.5 M NaCl, 100 mM KCl, 3 mM $MgCl_2$, 1 mM DTT). Elution was performed by applying a linear gradient (60 mL) from 0 to 100% Buffer B-ethane diol (50 mM Tris-HCl pH 7.5, 30% ethane diol (v/v), 100 mM KCl, 3 mM $MgCl_2$, 1 mM DTT). Eluted fractions containing AtCaM1/Ca^{2+}-dependent NADK activity were supplemented with 1 mM NAD^+ and immediately frozen. Fractions were pooled (5.6 mg, 2.32 µmol h^{-1} mg^{-1}, 8 mL) before loading onto a 1-mL CaM-Sepharose column (Stratagen) equilibrated with buffer C (50 mM Tris pH 7.5, 10% (v/v) glycerol, 1 mM DTT, 2 mM $CaCl_2$). The column was washed with 10 volumes Buffer C supplemented with 500 mM NaCl. Bound proteins were then eluted with 50 mM Tris pH 7.5, 10% (v/v) glycerol, 1 mM DTT and 5 mM EGTA. The fraction with highest activity (3 µg, 100 µl, 577 µmol h^{-1} mg^{-1}) was used for LC-MS/MS analyses (Fig. S1).

Mass spectrometry-based proteomic analyses

Proteins from the eluate and flow-through fractions were stacked by performing a very short run on an SDS-PAGE gel (NuPAGE 4-12%, ThermoFisher Scientific). Proteins were revealed by staining with Coomassie blue (R250, Bio-Rad), and submitted to in-gel digestion using modified trypsin (Promega, sequencing grade), as previously described (Casabona et al., 2013).

Resulting peptides were analyzed by online nanoLC-MS/MS (UltiMate 3000 and LTQ23 Orbitrap Velos Pro, Thermo Scientific). Briefly, peptides were sampled on a 300 µm x 5 mm PepMap C18 precolumn and separated on a 75 µm x 250 mm C18 column (PepMap, Thermo Scientific). MS and MS/MS data were acquired using Xcalibur (Thermo Scientific). Peptides and proteins were identified using Mascot (version 2.6), performing concomitant searches against Uniprot (*A. thaliana* taxonomy), the classical contaminants database (in-house) and the corresponding reversed databases. Proline software (http://proline.profiproteomics.fr) was used to filter the results (conservation of rank 1 peptides, peptide identification FDR < 1% as calculated on peptide scores using the reverse database strategy, minimum peptide score of 25, and minimum of one specific peptide identified per protein group). Results from individual samples were compiled, and grouped before comparing protein groups from different samples. Proteins were considered to be enriched in the eluate if they were identified only in this sample with a minimum of five specific spectral counts, or if they were enriched at least 10-fold in this sample compared to flow-through sample. Relative quantification was performed on the basis of specific spectral counts.

Recombinant protein expression and purification

Full-length At1g04280 cDNA was amplified by PCR from a pYES cDNA library (Elledge et al., 1991) using the primers listed in Supplemental Table S2. The PCR products digested by Nde I and Xho I were ligated into a pet28b(+) vector digested by the same enzymes to produce the constructs named pet28(b)-6HIS-NADKc and pet28(b)-6HIS-Δ38NADKc. The proteins were produced from these constructs with a 22-amino-acid N-terminal His-tag.

Rosetta2-competent cells were transformed by one or the other of these two constructs and grown at 37 °C in the presence of Chloramphenicol (34 μg.mL-1) and Kanamycin (50 μg.mL^{-1}) until Abs at 600 nm reached 0.6. IPTG (0.4 mM) was added, and growth was continued at 20 °C for 15 h. Bacteria were pelleted, suspended in Buffer D (50 mM HEPES pH 7.8, 500 mM KCl, 10% (v/v) glycerol, 50 mM L-arginine, 50 mM L-glutamate, 1 mM NAD^+) supplemented with 1 mM benzamidine and 5 mM ε-aminocaproic acid, 1 mM β-mercaptoethanol, and lysed by sonication. Insoluble material was removed by centrifugation (15,000 g, 20 min, 4 °C), and soluble proteins were recovered. A much higher production level and higher activity were obtained with the 6HIS-Δ38-NADKc construct, therefore further work was performed with this protein. The protein extract (30 mL, 11.3 mg mL^{-1}) was loaded onto a Ni-NTA Sepharose column (3 mL resin). After washing with buffer D supplemented with 50 mM imidazole (15 mL), the recombinant protein was eluted in buffer A supplemented with 250 mM imidazole. The imidazole concentration was reduced to 5 mM by protein-concentration cycles followed by dilution in buffer A. Pooled fractions containing NADKc activity were concentrated on 10K Vivascience concentrators, aliquoted, frozen in liquid N_2 and stored at -80 °C. After this first purification step, the protein fraction still contained small amounts of contaminating proteins. To improve purification, Ni-NTA-Sepharose fractions (2 mg, 2.2 mL) were denatured in 8 M urea and purified on Ni-NTA Sepharose under denaturing conditions (6 M urea). After washing with 15 mL buffer E (25 mM Tris-Cl pH 8.0, 500 mM NaCl, 5 mM β-mercaptoethanol, 6 M urea) supplemented with 50 mM imidazole, the pure denatured protein was eluted in buffer E supplemented with 250 mM imidazole. The denatured protein (0.3 mL, 0.3 mg, lane 4, Fig. S4) was then refolded by drop-by-drop dilution in 15 mL buffer D supplemented with 1 mM DTT. The refolding reaction was performed with mixing and at room temperature. The highly purified protein (lane 5, Fig. S4) was then concentrated as described above, aliquoted, frozen in liquid nitrogen and stored at -80 °C.

A. thaliana Calmodulin 1 (AtCaM1, At5g37780) was purified as previously described (Dell'Aglio et al., 2013a).

Proteins were quantified by the Bradford method, using bovine γ-globulin as a standard or, for purified proteins, by measuring A205nm (Scopes, 1974). CaM-binding peptide

(QKVPKLKDFVMAATRKQRFERVTKDLKVKR) was synthesized by Smart Bioscience (France). The control peptide sequence was VKDTELAKKVWDFSTKLTDS (Dell'Aglio, 2013[b]).

Activity measurements

NADK activity in extracts prepared from Col-0 *A. thaliana* plants, *K. flaccidum*, *M. polymorpha* and *C. reinhardtii* was measured at 25 °C as previously described (Turner et al., 2004) in the presence of a CaM inhibitor (trifluoroperazine, 50 µM) or in the presence of AtCaM1 (1 µM) and Ca^{2+} (500 µM) . Recombinant NADKc activity was measured in thermostatic cuvettes (25 °C) with 20 nM enzyme in the presence of 50 mM HEPES-KOH pH 7.8, 5 mM glucose-6-phosphate, 10 mM $MgCl_2$ and variable concentrations of NAD^+ and ATP (or other nucleotide), 30 mU of glucose-6-phosphate dehydrogenase from baker's yeast and, where indicated in the figure legends, 50 µM Ca^{2+} and/or AtCaM1. NADPH production was detected by monitoring absorbance at 340 nm ($\varepsilon_{340\ nm}$ = 6250 M^{-1} s^{-1}). Kinetic data reported in Table 1 were calculated by fitting enzymatic data to the appropriate theoretical equations using the Kaleidagraph program (Synergy Software, Reading, PA, USA). Tight binding of AtCaM1 onto NADKc was fitted using Eqn. 1:

$$v/[E]0 = k\text{cat}\frac{([\text{CaM}] + k\text{d} + [\text{E}]0) - \sqrt{([\text{CaM}] + k\text{d} + [\text{E}]0)^2 - 4 * \ k\text{d} * [\text{E}]0}}{2[\text{E}]0}$$

(Eqn.1)

where *k*cat is the catalytic constant for NADKc, [CaM] is the total CaM concentration, *k*d is the dissociation constant for the interaction between CaM and NADKc, and [E]0 is the total NADKc concentration.

Subcellular localization by confocal microscopy

The N-ter of the protein (amino acids: 1-60) or the entire protein sequence was amplified by PCR from pet28(b)-6HIS-NADKc using the primers listed in Supplemental Table S2. The amplified PCR products were cloned into the Gateway-adapted vector pDONR211 by BP recombination, to produce pDONR:NADKc$_{Nter}$, pDONR:NADKc and pDONR:NADKc$_{STOP}$ constructs.

These vectors were then recombined with pB7YWG2,0 and pB7WGY2,0 vectors (Karimi et al., 2007), respectively, to generate pB7YWG2:NADKc$_{Nter}$-YFP, pB7YWG2:NADKc-YFP and pB7WGY2:YFP-NADKc through the LR recombination reaction. All vectors were transformed into *Agrobacterium tumefaciens* C58 and used for tobacco leaf infiltration.

Transient expression in *Nicotiana benthamiana* var. Xanthi was performed by infiltrating leaves with a suspension of *A. tumefaciens* harboring pB7YWG2:NADKc$_{Nter}$-YFP and RFP fused with the first 69 amino acids of ATP synthase subunit 9a mitochondrial marker (pSu9–RFP) (Michaud et al., 2014) or pB7WGY2:YFP:NADKc, and the silencing suppressor P19 protein.

Transformed samples were observed by confocal microscopy on a LSM 800 confocal microscope equipped with a Plan-Apo 63X/1.4 oil DIC lens, two GaAsP detectors and one Airyscan detector. YFP and RFP fluorophores were excited at 488 and 558 nm, respectively, and emission signals were measured at 488-560 nm for YFP, and at 568-611 nm for RFP.

Stable expression in *Arabidopsis thaliana* seedlings was achieved by transforming the localization vectors into *A. tumefaciens* C58, which was used for floral dipping transformation. Complemented lines were screened based on their BASTA-resistance.

Confocal microscopy analyses of stable transgenic Arabidopsis seedlings root and shoot cells were performed using a Nikon Eclipse Ti2 inverted microscope, equipped with a Nikon A1+ laser scanning device (Nikon). Images were acquired by a CFI Apochromat TIRF 100XC, 1.49 N.A., oil immersion. EGFP or YFP were excited with the 488 nm laser and the emission was collected at 525-550 nm. For co-localization studies with Tetramethylrhodamine, Methyl Ester, Perchlorate (TMRM) seedlings were dipped in the following solution: 10 mM MES, 5 mM KCl, 10 mM $CaCl_2$, pH 5.8 with TRIS-base supplemented with 500 nM TMRM. TMRM was excited with the 561 nm laser and the emission was collected at 570-620 nm. Chlorophyll was excited with the 488 nm laser and the emission was collected at 663-738 nm. Pinhole was set to 0.6 (Figure 2A to F) or 0.8 (Figure 2G-O) airy unit and the images were acquired using 2048 x 2048 pixels. Pixel intensities of the YFP and TMRM fluorescences were extracted using FIJI software (https://fiji.sc/).

Measurement of photosynthetic parameters

Maximum quantum yield of photosystem II (F_V/F_M), relative electron transport rate (ETR) and non-photochemical quenching (NPQ) were determined using a chlorophyll fluorescence imaging system (SpeedzenIII, JbeamBio, France) Fv/Fm: (Fm-F_O)/Fm; ETR = ((F_M' – F_S)/F_M'); NPQ = (F_M – F_M')/F_M'; where F_M = maximum fluorescence; F_O = minimum fluorescence; F_V =variable fluorescence (F_V = F_M – F_O) in dark-adapted state (Maxwell and Johnson, 2000). F_M', maximum fluorescence in the light; F_S, steady-state chlorophyll fluorescence. Plants were dark adapted for at least 30 minutes prior to measurement.

Mutant complementation

To complement the SALK_006202 NADKc mutant line, the entire NADKc protein sequence was amplified by PCR from pet28(b)-6HIS-NADKc using the primers listed in Supplemental Table S1. The amplified PCR product was cloned into the Gateway-adapted vector pDONR211 by BP recombination, thus generating pDONR:NADKcSTOP. This vector was then recombined with pB2GW7,0 (Karimi et al., 2007) to generate pB2GW7:NADKc by the LR recombination reaction. This vector was transformed into *A. tumefaciens* C58 and used for floral dipping transformation. Complemented lines were screened based on their BASTA-resistance and AtCaM1/Ca^{2+}- dependent NAD^+ kinase activity.

Lines for which levels of AtCaM1/Ca^{2+}-dependent NAD^+ kinase activity were similar to wild-type plants were further analyzed.

NAD(P)$^+$ measurements

NAD(P)(H) cycling assays were adapted from Gibon and Larher (1997). All reagents were from Sigma. *A. thaliana* plantlets were grown for seven days in continuous light (Benamar A, 2013) then challenged for 12 min. with flg22 (1 µM) as previously described (Bisceglia & Savatin, 2015). Seedlings were harvested in pools of 80-100 mg each and immediately frozen in liquid nitrogen. Reduced and oxidised forms were extracted with 100 mM NaOH and 100 mM HCl respectively, and heated at 95°C for 5 min. After cooling down, tubes were centrifuged at 10,000 g for 10 min. Then 5 µl of the supernatant were transferred to flat bottom polystyrene microplates (Greiner), neutralised with 5 µl of 100 mM HCl

(reduced forms) or 100 mM NaOH (oxidised forms), and 90 µl of determination mix added. For NAD(H) measurements, final concentrations of the reagents were 100 mM Tricine/KOH buffer, pH 9.0, 10 mM $MgCl_2$, 8 mM EDTA, 1% v/v ethanol, 1 mM thiazolyl blue, 0.5 mM phenazine ethosulfate and 20 units·ml^{-1} alcohol dehydrogenase (Merck). For NADP(H) measurements, final concentrations of the reactants were 100 mM Tricine/KOH buffer, 10 mM $MgCl_2$, 8 mM EDTA, 5 mM glucose-6-phosphate, 1 mM thiazolyl blue, 0.5 mM phenazine ethosulfate and 10 units·ml^{-1} glucose-6-phosphate dehydrogenase grade I (Merck). Changes in absorbance were read at 570 nm in an MP96 reader (SAFAS) until stabilised. For each coenzyme form and/or each microplate a standards curve ranging from 0 to 40 pmol per well was used; blanks without enzyme were also recorded in order to subtract interferences coming from the extracts. Results are expressed as the average obtained for 3 independent extracts.

Oxidative burst measurements

A. thaliana plantlets were grown for 7 days in continuous light (Benamar et al., 2013) and immunity-related accumulation of H_2O_2 following stimulation with flg22 (1 µM) was analyzed as previously described (Bisceglia & Savatin, 2015). The purity of the flg22 peptide (synthetized by GENECUST, Boynes, France) was estimated at 96.14%. Luminescence measurements were performed with a microplate reader SPARK 10M (TECAN) using 96-well microtiter plates (flat bottom, white, Greiner). For each plant type, results are expressed as the average luminescence obtained for 4 wells (*i.e.*, 120 plantlets).

Molecular Phylogenetic analysis by the Maximum Likelihood method

Protein sequences of NADKc-like proteins were retrieved from the Phytozome website (Goodstein et al., 2012), with some exceptions. The sequences of *U. mutabilis* and *C. braunii* were retrieved from the ORCAE project website (Sterck et al., 2012) and those of *S. minuta*, *E. fimbriata*, Mougeotia sp. and Spirogyra sp. were retrieved from the One KP project website (Matasci et al., 2014). The evolutionary history of NADKc was inferred by using the Maximum Likelihood method, based on the JTT matrix-based model (Jones et al., 1992). The tree with the highest log-likelihood (-31386.44) is shown. The

percentage of trees produced in which the associated taxa clustered together is shown next to the branches. Initial tree(s) for the heuristic search were obtained automatically by applying Neighbor-Join and BioNJ algorithms to a matrix of pairwise distances estimated using a JTT model, and then selecting the topology with the highest log-likelihood value. A discrete Gamma distribution was used to model evolutionary rate differences between sites (5 categories (+G, parameter = 0.9891)). The tree is drawn to scale, with branch lengths based on the number of substitutions per site. The analysis involved 45 amino acid sequences. There were a total of 1196 positions in the final dataset. Evolutionary analyses were performed in MEGA7 (Kumar et al., 2016).

Supplemental references

Benamar A, Pierart A, Baecker V, Avelange-Macherel M, Rolland A, Gaudichon S, di Gioia L, Macherel, D (2013) Simple system using natural mineral water for high-throughput phenotyping of *Arabidopsis thaliana* seedlings in liquid culture. International Journal of High Throughput Screening **4:** 1-15

Bisceglia NG, Gravino M, Savatin DV (2015) Luminol-based Assay for Detection of Immunity Elicitor-induced Hydrogen Peroxide Production in *Arabidopsis thaliana* Leaves. BioProtocols **5:** 1-7

Casabona M, Vandenbrouck Y, Attree I, and Couté Y (2013) Proteomic characterization of *Pseudomonas aeruginosa* PAO1 inner membrane. Proteomics **13:** 2419-2423

Dell'Aglio E, Giustini C, Salvi D, Brugière S, Delpierre F, Moyet L, Baudet M, Seigneurin-Berny D, Matringe M, Ferro M, et al (2013[a]) Complementary biochemical approaches applied to the identification of plastidial calmodulin-binding proteins. Mol Biosyst **9:** 1234-1248

Dell'Aglio E (2013[b]) The regulation of plastidial proteins by calmodulins. Université de Grenoble

Elledge SJ, Mulligan JT, Ramer SW, Spottswood M, Davis RW (1991) Lambda YES: a multifunctional cDNA expression vector for the isolation of genes by complementation of yeast and Escherichia coli mutations. Proc Natl Acad Sci USA **88:** 1731-1735

Gibon Y, Larher F (1997) Cycling assay for nicotinamide adenine dinucleotides: NaCl precipitation and ethanol solubilization of the reduced tetrazolium. Analytical Biochemistry **251:** 153-157

Goodstein DM, Shu SQ, Howson R, Neupane R, Hayes RD, Fazo J, Mitros T, Dirks W, Hellsten U, Putnam N, et al (2012) Phytozome: a comparative platform for green plant genomics. Nucleic Acids Research **40:** D1178-D1186

Jones D, Taylor W, Thornton J (1992) The rapid generation of mutation data matrices from protein sequences. Comput Appl Biosci **8:** 275-282

Karimi M, Depicker A, Hilson P (2007) Recombinational cloning with plant Gateway vectors. Plant Physiol **145:** 1144-1154

Kumar S, Stecher G, Tamura K (2016) Molecular evolutionary genetics analysis version 7.0 for bigger datasets. Mol Biol Evol **33**

Matasci N, Hung LH, Yan ZX, Carpenter EJ, Wickett NJ, Mirarab S, Nguyen N, Warnow T, Ayyampalayam S, Barker M, et al (2014) Data access for the 1,000 Plants (1KP) project. Gigascience **3**

Michaud M, Ubrig E, Filleur S, Erhardt M, Ephritikhine G, Maréchal-Drouard L, Duchêne A-M (2014) Differential targeting of VDAC3 mRNA isoforms influences mitochondria morphology. Proc Natl Acad Sci USA **111:** 8991-8996

Murashige T, Skoog F (1962) A revised medium for rapid growth of bioassays with tobacco tissue culture. Physiol Plant **15:** 473-497

Scopes RK (1974) Measurement of protein by spectroscopy at 205 nm. Anal. Biochem. **59:** 277-282

Sun Y, Li L, Macho AP, Han Z, Hu Z, Zipfel C, Zhou JM, Chai J. (2013) Structural basis for flg22-induced activation of the Arabidopsis FLS2-BAK1 immune complex. Science **342:** 624-8

Sterck L, Billiau K, Abeel T, Rouze P, van de Peer Y (2012) ORCAE: online resource for community annotation of eukaryotes. Nature Methods **9:** 1041-1041

Turner WL, Waller JC, Vanderbeld B, Snedden WA (2004) Cloning and characterization of two NAD kinases from Arabidopsis. Identification of a calmodulin binding isoform. Plant Physiol **135:** 1243-1255

Supplemental Figures Legend

Supplementary Figure S1. CaM-affinity purification of native CaM-dependent NAD^+ kinase from Arabidopsis plantlets. Proteins loaded and eluted from the CaM affinity chromatography column were separated by SDS-PAGE and stained with silver nitrate. In the "Loaded fraction", 24 µg in 38 µl were loaded; in the washings and EGTA elution fractions, 38 µl of each fraction were loaded (concentration not determined). Mass spectrometry-based proteomics was used to identify proteins strongly enriched in the EGTA elution compared to the Ca^{2+}-containing washing steps (Supplemental Table S1). Protein bands analysed by mass spectrometry are included in red boxes.

Supplementary Fig. S2. Features of NADKc primary sequence and its homologues in other plant and algae species. (A) putative CaM binding site (*A. thaliana* NADKc amino acids 167-200). Red residues are those constituting the 1-5-8-14 motif. This domain is not conserved in *C. subellipsoidea*, *U. mutabilis* and *S. minuta*. *A. thaliana*: *Arabidopsis thaliana*, *S. phallax*: *Sphagnum phallax*, *P. patens*: *Physcomitrella patens*, *M. polymorpha*: *Marchantia polymorpha*, *S. mollendorffii*: *Selaginella mollendorffii*, *S. lycopersicum*: *Solanum lycopersicum*, *G. max*: *Glycine max*, *M. truncatula*: *Medicago truncatula*, *P. trichocarpa*: *Populus trichocarpa*, *M. acuminata*: *Musa acuminata*, *O. sativa*: *Oryza sativa*, *B. distachyon*: *Brachypodium distachyon*, *S. italica*: *Setaria italica*, *Z. mays*: *Zea mays*, *C. subellipsoidea*: *Coccomyxa subellipsoidea*, *U. mutabilis*: *Ulva mutabilis*, *S. minuta*: *Spirotaenia minuta*, *K. flaccidum*: *Klebsormidium flaccidum*, *E. fimbriata*: *Entransia fimbriata*. (B) Walker A motif (in red, residues characterizing the motif; *A. thaliana* NADKc amino acids 236-250). For gene references, see the legend of Fig. S6.

Supplementary Fig. S3. Purification of recombinant NADKc produced in *E. coli*. 6HIS-Δ38NADKc was purified as indicated in Material and Methods. Lane 1: Rosetta2 soluble extract transformed with empty pET28a (40 µg); lane 2: Rosetta2 soluble extract transformed with pET28a6HIS-Δ38NADKc (40

µg); lane 3: Ni-NTA pool (10 µg); lane 4: urea-denatured 6HIS-Δ38NADKc purified on Ni-NTA (10 µg); lane 5: refolded 6HIS-Δ38NADKc (2 µg).

Supplementary Fig. S4. $NADKc_{Nter}$-YFP associates with mitochondria in tobacco leaves. Representative pictures of transiently transformed tobacco leaf cells. Left: YFP (green), Center: RFP (red), and Right: merged fluorescence. The top row shows a representative image of tobacco cells co-transformed with the $NADKc_{Nter}$-YFP construct and a mitochondrial marker, pSu9– RFP. The middle row shows a close-up of mitochondria from the lower right region of the images in the top row (white boxes). White arrows indicate regions in which the YFP signal appears peripheral with respect to the RFP signal. The bottom row shows a representative image of tobacco cells transformed with the YFP-NADKc construct alone. The central image shows the background signal in the RFP channel. White bars represent 2 µm in the upper and middle row, and 10 µm in the lower row.

Supplementary Fig. S5. Phenotype of *nadkc* mutants. (A) 21-day-old plants grown under long day photoperiod (16 h light/8 h dark); (B) 28-day-old plants grown under short day photoperiod (8 h light/16 h dark). (C-E) Photosynthetic parameters in Col-0 and *nadkc* plants: (C) NPQ, (D) Fv/Fm and (E) electron transport rate.

Supplementary Fig. S6. Phylogeny of NADKc. Maximum likelihood phylogenetic tree of NADKc-like proteins in the following plant and algal species: *Arabidopsis thaliana* (*A. thaliana*), *Populus trichocarpa* (*P. trichocarpa*), *Manihot esculenta* (*M. esculenta*), *Gossypium raimondii* (*G. raimondii*), *Solanum lycopersicum* (*S. lycopersicum*), *Setaria italica* (*S. italica*), *Zea mays* (*Z. mays*), *Oryza sativa* (*O. sativa*), *Brachypodium distachyon* (*B. distachyon*), *Musa acuminata* (*M. acuminata*), *Marchantia polymorpha* (*M. polymorpha*), *Physcomitrella patens* (*P. patens*), *Sphagnum phallax* (*S. phallax*), *Selaginella mollendorffii* (*S. mollendorffii*) *Klebsormidium flaccidum* (*K. flaccidium*), *Coccomyxa subellipsoidea* (*C. subellipsoidea*), *Ulva mutabilis* (*U. mutabilis*), *Spirotaenia minuta* (*S. minuta*), Mougeotia sp., Spirogyra sp. and *Entransia fimbriata* (*E. fimbriata*). Accession numbers: *A. thaliana-1* (NADKc): At1g04280, *A. thaliana-2*: At1g06750, *A. thaliana-3*: At2g30630, *P. trichocarpa-1*: Potri.008G162000, *P. trichocarpa-2*: Potri.002G043000, *P. trichocarpa-3*: Potri.005G220000, *P. trichocarpa-4*: Potri.008G162400, *M. esculenta-1*: Manes.15G036900, *M. esculenta-2*: Manes.03G168900, *M. esculenta-3*: Manes.01G200600, *M. esculenta-4*: Manes.05G086200, *G.*

raimondii-1: Gorai.011G171100, *G. raimondii-2*: Gorai.006G246600, *G. raimondii-3*: Gorai.004G074100, *G. raimondii-4*: Gorai.013G104300, *S. lycopersicum-1*: Solyc06g053810, *S. lycopersicum-2*: Solyc06g031670, *S. lycopersicum-3*: Solyc08g059750, *S. italica-1*: Seita.9G163700, *S. italica-2*: Seita.3G185100, *S. italica-3*: Seita.5G337000, *Z. mays-1*: GRMZM2G070252, *Z. mays-2*: GRMZM2G368410, *O. sativa-1*: Os03g43010, *O. sativa-2*: Os05g43300, *O. sativa-3*: Os01g56764, *B. distachyon-1*: Bradi1g14307, *B. distachyon-2*: Bradi2g51490, *B. distachyon-3*: Bradi2g20400, *M. acuminata-1*: SMUA_Achr5T03210, *M. acuminata-2*: GSMUA_Achr7T01560, *M. polymorpha*: Mapoly0142s0012, *P. patens*: Pp3c2_3490V3, *S. phallax-1*: Sphallax0059s0037, *S. phallax-2*: Sphallax0011s0002, *S. phallax-3*: Sphallax0120s0019, *S. mollendorffii-1*: scaffold 73427, *S. mollendorfii-2*: scaffold 231175, *K. flaccidum*: kfl00274_0130, *C. subellipsoidea*: XP_005648203, *U. mutabilis*: UM028_0076.1, *S. minuta*: NNHQ_2000691, *Mougeotia*: ZRMT_2002068, *Spirogyra*: HAOX_2025158, *E. fimbriata*: BFIK_2025349. The tree is drawn to scale, with branch lengths measured in the number of substitutions per site (scale bar in the bottom-left corner). The numbers at the interior nodes are bootstrap percentages.

Supplementary Table S1. List of Arabidopsis proteins bound on CaM-affinity column in the presence of Ca^{2+} and eluted by EGTA identified by mass-spectrometry.

Supplementary Table S2. Primers used in this study.

Table 1: NADKc kinetic parameters

Substrate varied	Constant substrate	K_M (µM)	k_{cat} (s^{-1})	k_{cat}/K_M ($\mu M^{-1}.s^{-1}$)
ATP	NAD^+ (10 mM)	203(±30)	41(±2)	0.2
CTP	NAD^+ (10 mM)	283(±70)	42(±1)	0.15
GTP	NAD^+ (10 mM)	522(±135)	26(±1)	0.05
UTP	NAD^+ (10 mM)	207(±26)	29.5(±2)	0.14
NAD^+	ATP (8 mM)	147 (±17)	42(±2)	0.28
$NADH^+$	ATP (8 mM)	n.d.	n.d.	n.d.
$NAAD^+$	ATP (8 mM)	n.d.	n.d.	n.d.

n.d.: not detected

Table 2: Comparison of CaM-dependent NADK activity in different photosynthetic organisms.

	A. thaliana	*M. polymorpha*	*K. flaccidum*	*C. reinhardtii*
Total activity[a]	31.2(±2.8)	6.9(±0.7)	5.8(±0.3)	24.6(±1.4)
CaM/Ca^{2+}-independent activity[b]	1.0(±0.3)	1.0(±0.1)	1.8(±0.3)	29.7(±2.7)
CaM/Ca^{2+}-dependent activity[c]	30.2	5.9	4.0	n.d.

n.d.: not detected.

Figure 1

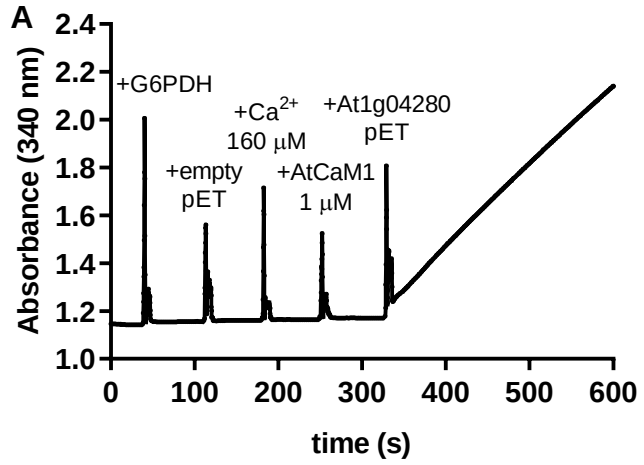
A
Absorbance (340 nm)
time (s)
+G6PDH
+empty pET
+Ca2+ 160 µM
+AtCaM1 1 µM
+At1g04280 pET

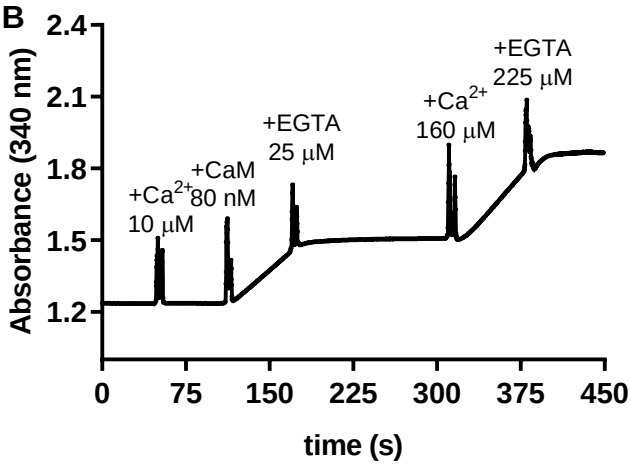
B
Absorbance (340 nm)
time (s)
+Ca2+ 10 µM
+CaM 80 nM
+EGTA 25 µM
+Ca2+ 160 µM
+EGTA 225 µM

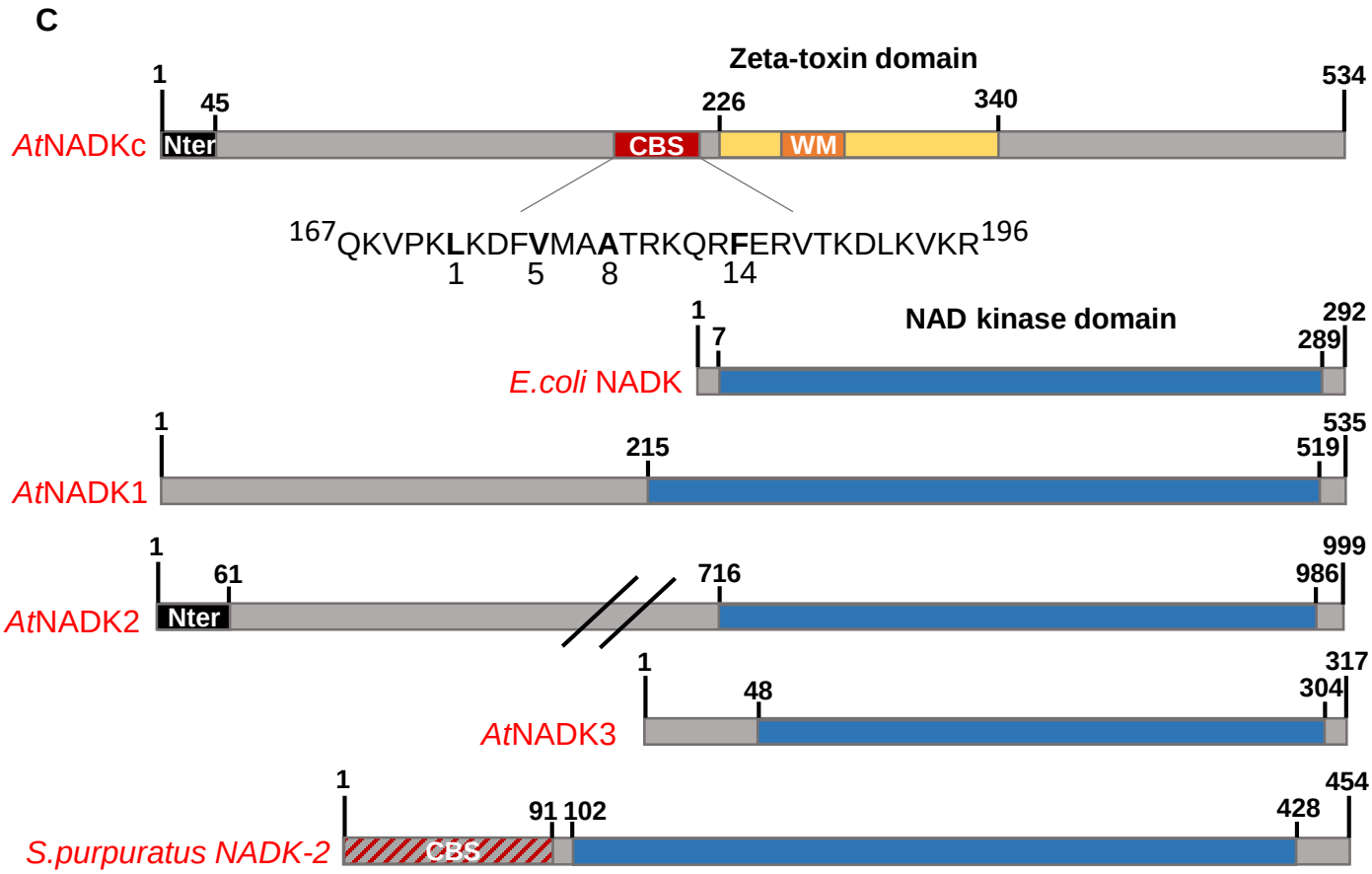
C
Zeta-toxin domain
AtNADKc
Nter
CBS
WM
167QKVPKLKDFVMAATRKQRFERVTKDLKVKR196
NAD kinase domain
E.coli NADK
AtNADK1
AtNADK2
AtNADK3
S.purpuratus NADK-2

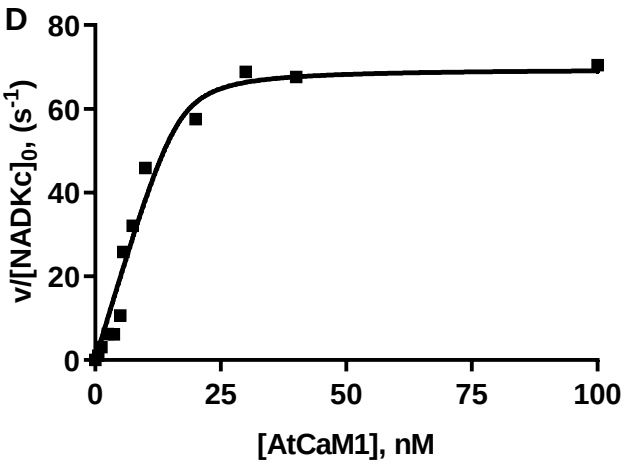
D
v/[NADKc]0, (s-1)
[AtCaM1], nM

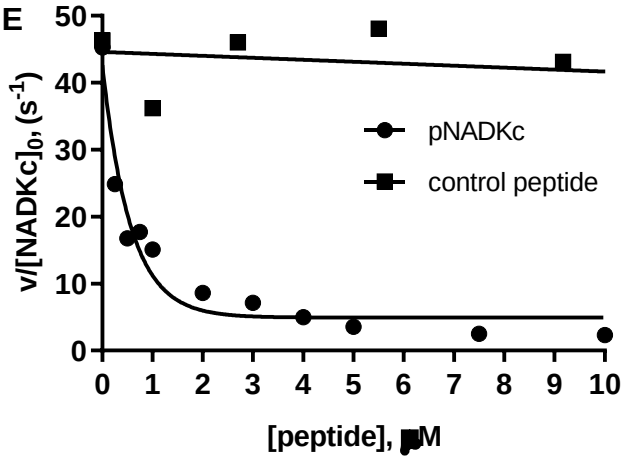
E
v/[NADKc]0, (s-1)
pNADKc
control peptide
[peptide], µM

Figure 1. Biochemical properties of a CaM-dependent NAD^+ kinase identified in Arabidopsis. (A) NAD^+ kinase activity measured in an *E. coli* extract expressing an empty pET28b(+) and an *E. coli* extract expressing At1g04280. Spikes correspond to the moments of addition of glucose 6-phosphate dehydrogenase (G6PDH), Ca^{2+}, AtCaM1, and *E. coli* extracts (10 μg). (B) NAD^+ kinase activity in an *E. coli* bacterial extract expressing At1g04280. Ca^{2+}, AtCaM1 and EGTA were added at different times, as indicated in the graph. (C) Schematic representation of the NADKc primary sequence and comparison with previously known NAD^+ kinases. Yellow: zeta-toxin domain (InterPro Homologous superfamily: IPR010488); black: N-terminal region with putative organelle target sequence; red: putative conserved Type A 1-8-14 CaM-binding site (detailed below the scheme); orange: Walker A motif (ATP-binding site); blue: NAD^+ kinase domain (InterPro Homologous Superfamily: IPR016064); red/grey: N-terminal sequence expected to contain a CaM-binding site according to Love et al, 2015. Sequences used for comparison (UniProt): *E. coli* NAD^+ kinase: P0A7B3; *A. thaliana* NAD^+ kinases: AtNADK1: Q56YN3; AtNADK2: Q9C5W3; AtNADK3: Q500Y9; *Strongylocentrotus purpuratus* NAD^+ kinase-2 (sea urchin CaM-dependent NAD^+ kinase, Love et al., 2015): C3RSF7. (D) Affinity of NADKc recombinant protein for AtCaM1: Activity of the purified NADKc recombinant protein after denaturation in urea and subsequent refolding was measured in the presence of 50 μM Ca^{2+} and as a function of [AtCaM1]. Experiments were performed in triplicate and data shown are from one representative experiment. Binding data were analysed assuming tight binding. K_d value for AtCaM1 binding varied from 0.6 to 1 nM. (E) Inhibition of NADKc activity by competition with the putative CaM-binding site (black dots). Black squares correspond to results obtained with a negative control peptide, which does not bind AtCaM1.

Figure 2

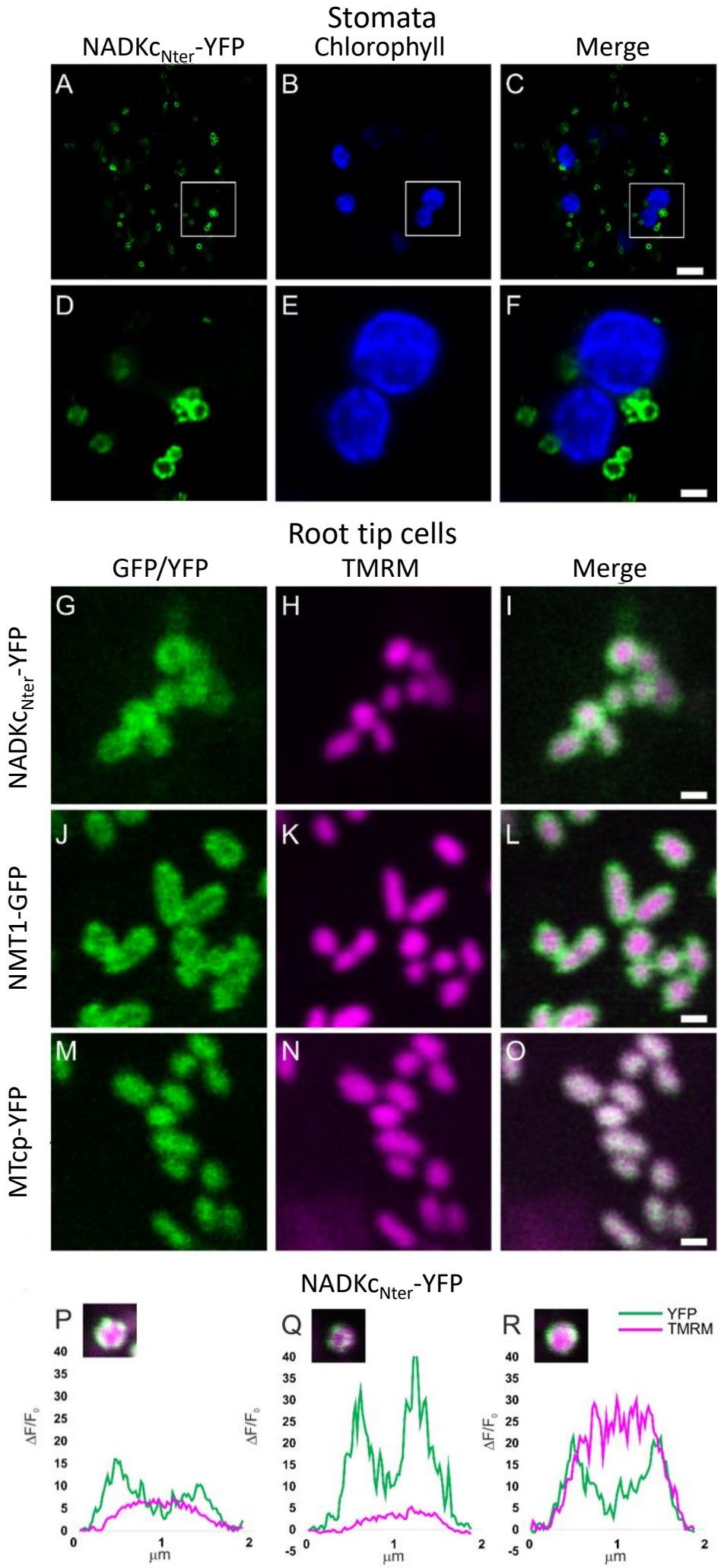
Stomata
NADKc$_{Nter}$-YFP
Chlorophyll
Merge
A
B
C
D
E
F
Root tip cells
GFP/YFP
TMRM
Merge
NADKc$_{Nter}$-YFP
NMT1-GFP
MTcp-YFP
G
H
I
J
K
L
M
N
O
NADKc$_{Nter}$-YFP
P
Q
R
YFP
TMRM
ΔF/F$_0$
µm

Figure 2. Analysis of submitochondrial localization of $NADKc_{Nter}$-YFP. (A to C) Confocal laser scanning microscopy images from stomata guard cells of a representative Arabidopsis seedling stably expressing $NADKc_{Nter}$-YFP. Scale bar = 5 µm. (D to E) Higher magnification of the region of interest shown in A to C (white squares). Scale bar = 1 µm. (A, D) YFP fluorescence in green; (B, E) chlorophyll fluorescence in blue; (C, F) merge between YFP and chlorophyll fluorescences. (G to I) Confocal laser scanning microscopy images from root tip cells of a representative Arabidopsis seedling stably expressing $NADKc_{Nter}$-YFP and stained with the mitochondrial matrix marker TMRM. Scale bar = 1 µm. (J to L) Confocal laser scanning microscopy images from root tip cells of a representative Arabidopsis seedling stably expressing NMT-GFP and stained with the mitochondrial matrix marker TMRM. Scale bar = 1 µm. (M to O) Confocal laser scanning microscopy images from root tip cells of a representative Arabidopsis seedling stably expressing MT-cpYFP and stained with the mitochondrial matrix marker TMRM. Scale bar = 1 µm. (G, M) YFP fluorescence in green; (J) GFP fluorescence in green; (H, K and N) TMRM fluorescence in magenta; (I, L and O) merge between YFP/GFP and TMRM fluorescences. NMT1-GFP and MT-cpYFP were used as markers for the mitochondrial outer mitochondrial membrane (OMM) and matrix, respectively. (P to R) Normalized pixel intensity distributions in the YFP and TMRM fluorescence channels plotted centrally across three individual mitochondria of a seedling expressing the $NADKc_{Nter}$-YFP.

Figure 3

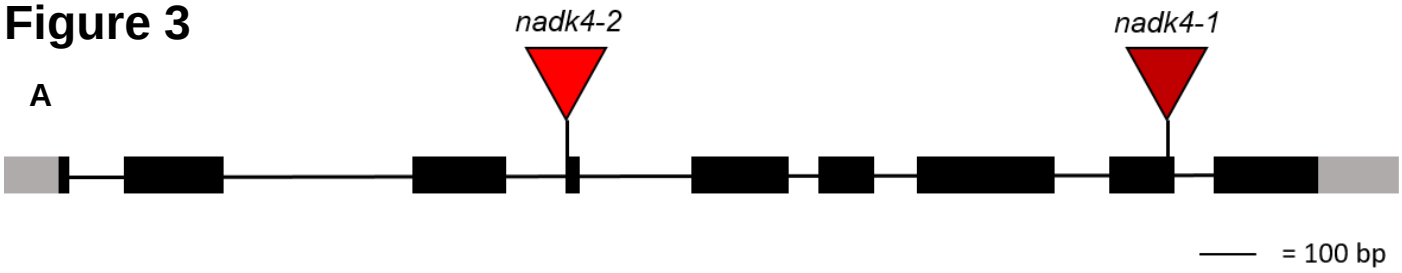
A
nadk4-2
nadk4-1
= 100 bp

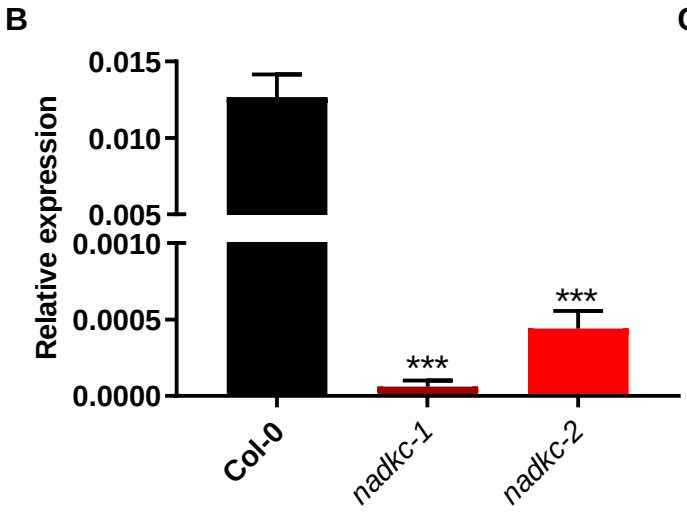
B
Relative expression
0.015
0.010
0.005
0.0010
0.0005
0.0000
***
***
Col-0
nadkc-1
nadkc-2

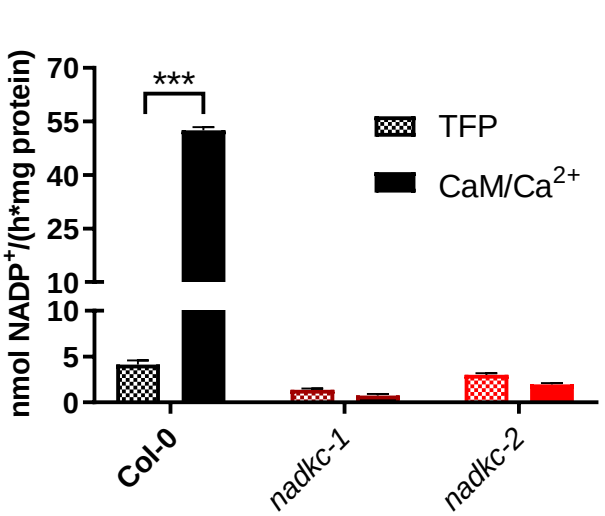
C
nmol NADP+/(h*mg protein)
70
55
40
25
10
10
5
0
***
TFP
CaM/Ca2+
Col-0
nadkc-1
nadkc-2

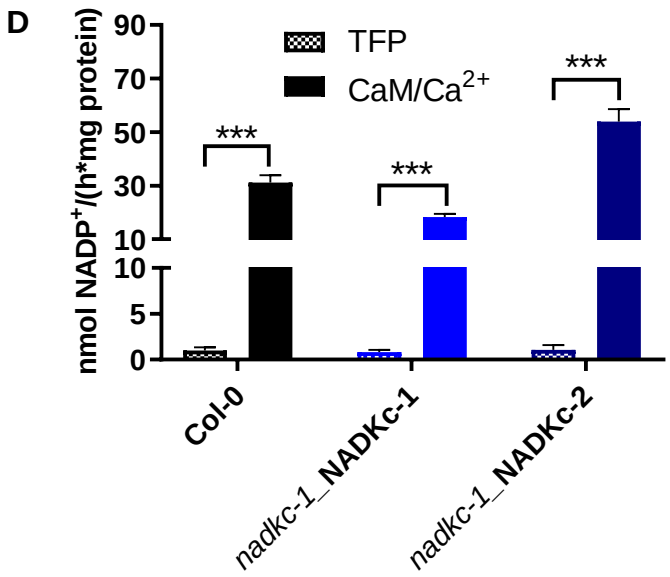
D
nmol NADP+/(h*mg protein)
90
70
50
30
10
10
5
0
***
***
***
TFP
CaM/Ca2+
Col-0
nadkc-1_NADKc-1
nadkc-1_NADKc-2

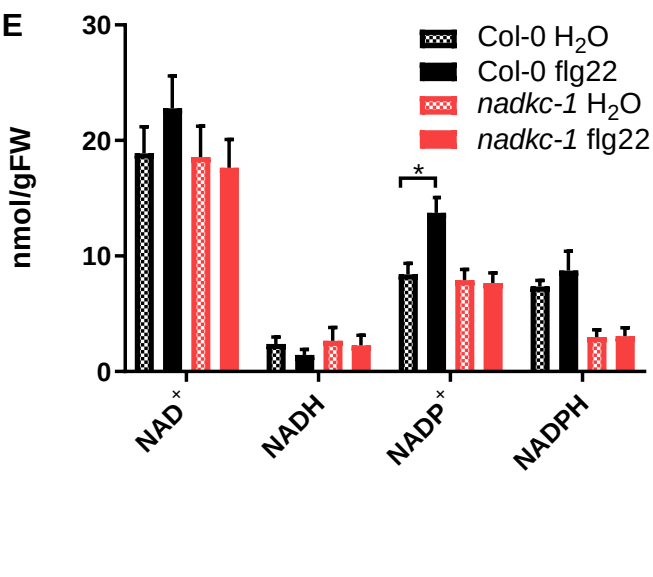
E
nmol/gFW
30
20
10
0
*
Col-0 H2O
Col-0 flg22
nadkc-1 H2O
nadkc-1 flg22
NAD+
NADH
NADP+
NADPH

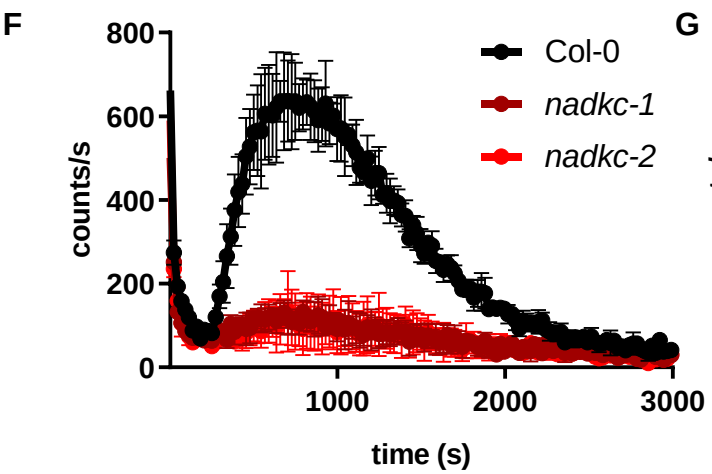
F
counts/s
800
600
400
200
0
1000
2000
3000
time (s)
Col-0
nadkc-1
nadkc-2

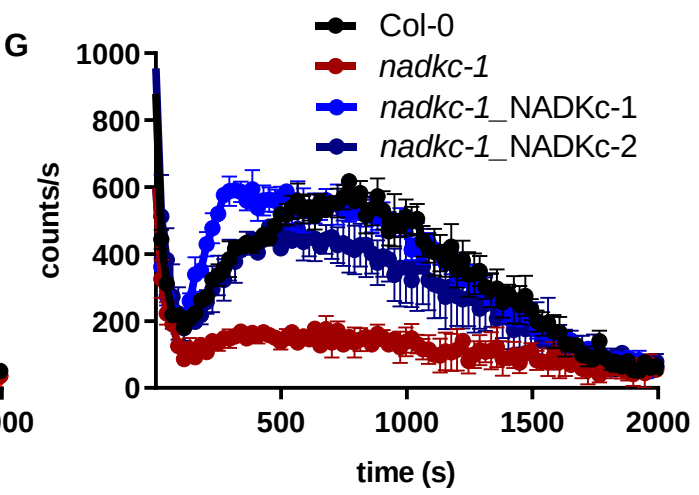
G
counts/s
1000
800
600
400
200
0
500
1000
1500
2000
time (s)
Col-0
nadkc-1
nadkc-1_NADKc-1
nadkc-1_NADKc-2

Figure 3. The CaM/Ca^{2+}-dependent NAD^+ kinase activity of Arabidopsis seedlings is absent in *nadkc* mutants. (A) schematic representation of the NADKc gene and position of the T-DNA insertions in the *nadkc-1* and *nadkc-2* mutant lines. (B) NADKc transcript levels in Col-0 and *nadkc*-mutant seedlings. Levels are expressed relative to GAPDH. Data shown correspond to mean +/- s.d., n=3. (C) NAD^+ kinase activity measured in Col-0 and *nadkc* mutant plants (7-day-old whole plantlets), in the presence of the CaM inhibitor TFP (40 μM) or AtCaM1 (250 nM) and Ca^{2+} (0.5 mM). Values correspond to the average of four replicates. (D) NAD^+ kinase activity measured in Col-0 and mutant plants complemented with NADKc gene (*nadkc-1*_NADKc-1 and *nadkc-1*_NADKc-2) in 7-day-old whole plantlets, in the presence of the CaM inhibitor TFP (40 μM) or of AtCaM1 (250 nM) and Ca^{2+} (0.5 mM). (E) $NAD(P)^+$ and NAD(P)H concentrations in 7-day-old seedlings exposed (flg22, 1 μM) or unexposed (H_2O) for 12 min. to the bacterial elicitor flagellin22. (80-100 mg of tissue per measure, data shown correspond to mean +/- s.e.m. for 3 biological replicates). (F) Flg22 (1 μM)-induced oxidative burst in 7-day-old Col-0 and *nadkc* mutant seedlings (30 plantlets per well, data shown correspond to mean +/- s.d. for 4 wells). (G) Flg22 (1 μM)-induced oxidative burst in Col-0, *nadkc-1* mutant and mutant plants complemented with NADKc gene (*nadkc-1*_NADKc-1 and *nadkc-1*_NADKc-2); 7-day-old seedlings, 30 plantlets per well. Data shown correspond to mean +/- s.d. for 4 wells. Asterisks indicate a significant difference between two conditions based on a Welch's t test (*$p < 0.05$; ***$p < 0.001$).

Figure 4

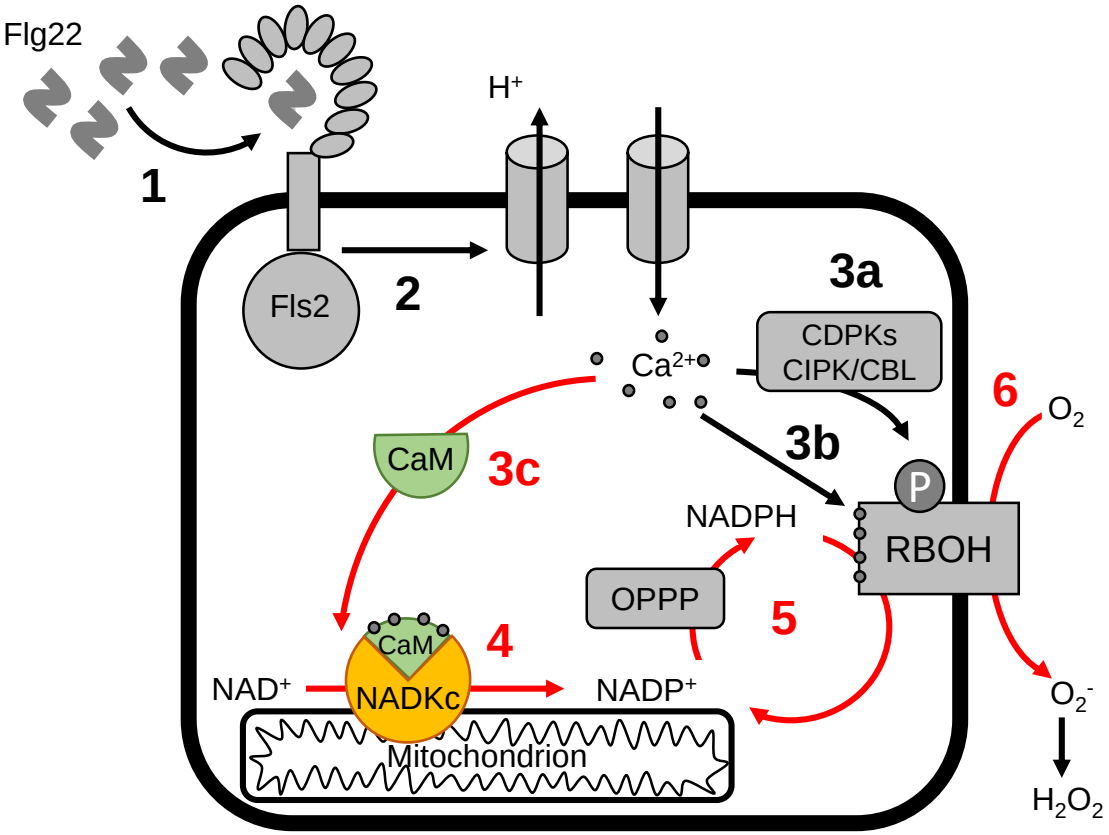
Flg22
1
H+
Fls2
2
3a
CDPKs
CIPK/CBL
Ca2+
6
O2
CaM
3c
3b
P
NADPH
RBOH
OPPP
5
CaM
4
NAD+
NADKc
NADP+
O2-
Mitochondrion
H2O2

Figure 4. Hypothetical model of the role of CaM/Ca^{2+}-dependent NADKc in sustaining the flg22-induced oxidative burst in Arabidopsis seedlings. Numbers refer to known sequential events; red numbers highlight events related to NADKc activation: 1. binding of Flg22 elicitor to the Fls2 receptor (Sun et al., 2013); 2. activation of proton efflux and Ca^{2+} influx; 3a. Ca^{2+}-dependent activation of CDPKs and CIPK/CBLs that phosphorylate RBOH proteins; 3b. Ca^{2+} binding to RBOH proteins; 3c. Ca^{2+} binding to CaM, leading to CaM structural modification and formation of the CaM/NADKc complex; 4. activation of $NADP^{+}$ production by NADKc; 5. increased flux in the oxidative pentose phosphate pathway (OPPP), leading to a higher availability of NADPH; 6. production of the extracellular oxidative burst by NADPH oxidases (RBOH proteins).

Figure S1

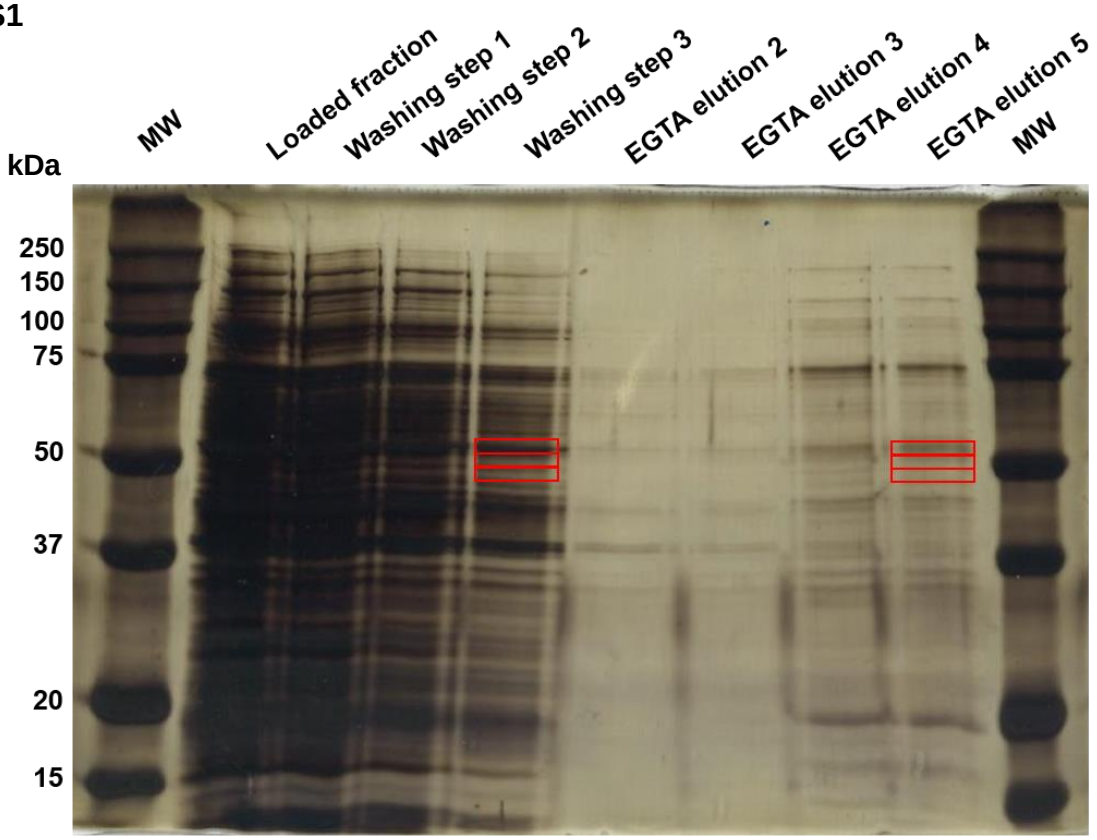

Supplemental Figure S1. CaM-affinity purification of native CaM-dependent NAD^+ kinase from Arabidopsis plantlets. Proteins loaded and eluted from the CaM affinity chromatography column were separated by SDS-PAGE and stained with silver nitrate. In the "Loaded fraction", 24 µg in 38 µl were loaded; in the washings and EGTA elution fractions, 38 µl of each fraction were loaded (concentration not determined). Mass spectrometry-based proteomics was used to identify proteins strongly enriched in the EGTA elution compared to the Ca^{2+}-containing washing steps (Supplemental Table S1). Protein bands analysed by mass spectrometry are included in red boxes.

Figure S2

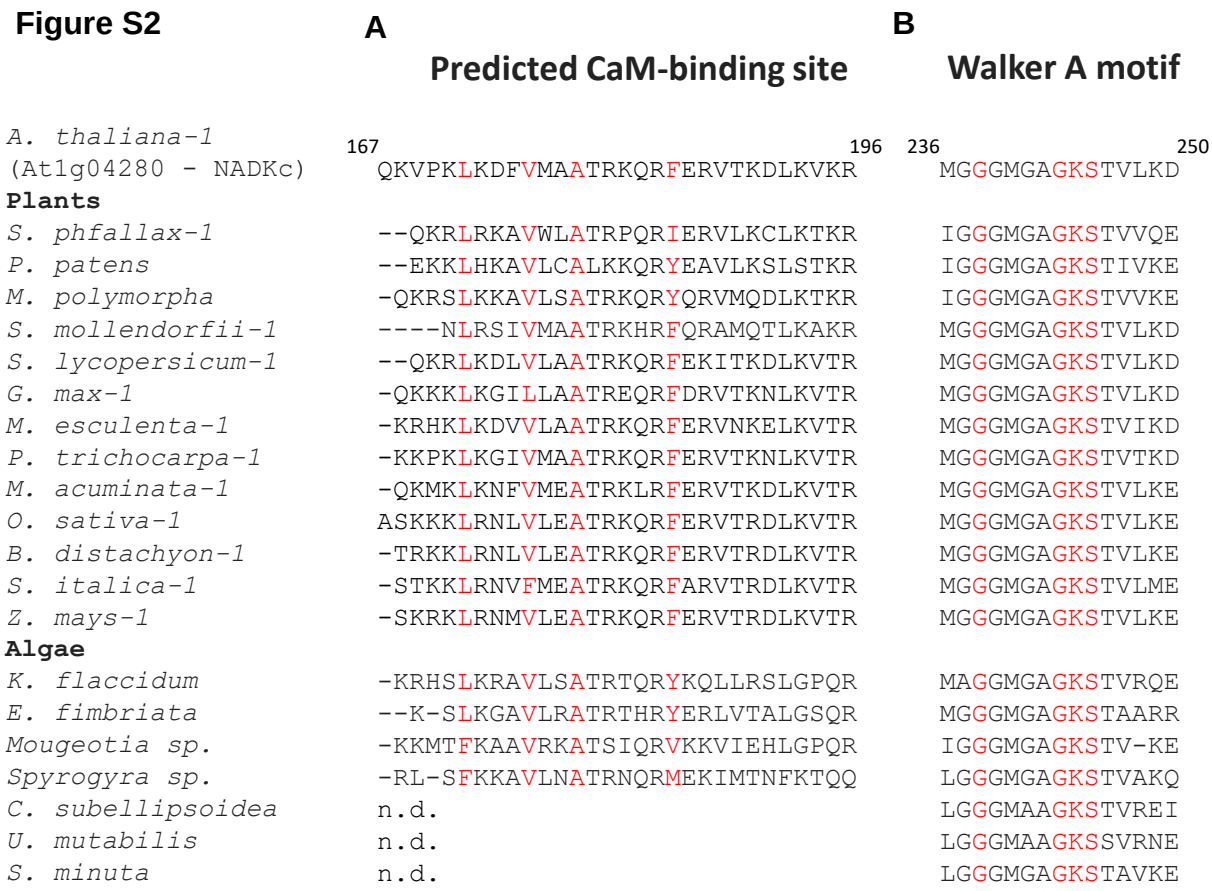

Supplemental Figure S2. Features of NADKc primary sequence and its homologues in other plant and algae species. (A) putative CaM binding site (Arabidopsis NADKc amino acids 167-200). Red residues are those constituting the 1-5-8-14 motif. This domain is not conserved in *C. subellipsoidea*, *U. mutabilis* and *S. minuta*. *A. thaliana*: *Arabidopsis thaliana*, *S. phallax*: *Sphagnum phallax*, *P. patens*: *Physcomitrella patens*, *M. polymorpha*: *Marchantia polymorpha*, *S. mollendorffii*: *Selaginella mollendorffii*, *S. lycopersicum*: *Solanum lycopersicum*, *G. max*: *Glycine max*, *M. truncatula*: *Medicago truncatula*, *P. trichocarpa*: *Populus trichocarpa*, *M. acuminata*: *Musa acuminata*, *O. sativa*: *Oryza sativa*, *B. distachyon*: *Brachypodium distachyon*, *S. italica*: *Setaria italica*, *Z. mays*: *Zea mays*, *C. subellipsoidea*: *Coccomyxa subellipsoidea*, *U. mutabilis*: *Ulva mutabilis*, *S. minuta*: *Spirotaenia minuta*, *K. flaccidum*: *Klebsormidium flaccidum*, *E. fimbriata*: *Entransia fimbriata*. (B) Walker A motif (in red, residues characterizing the motif; *A. thaliana* NADKc amino acids 236-250). For gene references, see the legend of Fig. S6.

Figure S3

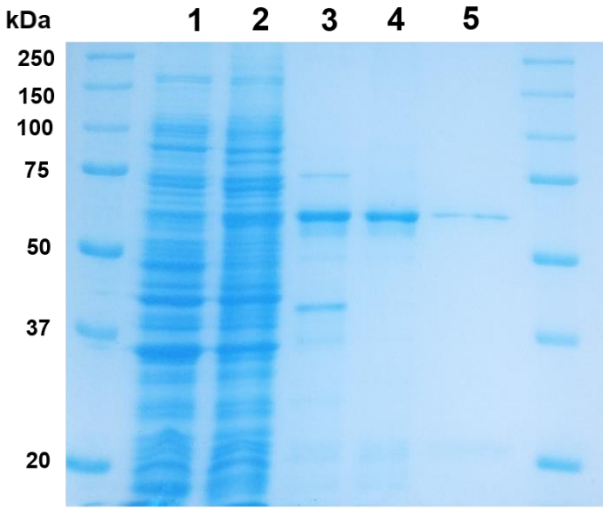

Supplemental Figure S3. Purification of recombinant NADKc produced in *E. coli*. 6HIS-Δ38NADKc was purified as indicated in Material and Methods. Lane 1: Rosetta2 soluble extract transformed with empty pET28a (40 µg); lane 2: Rosetta2 soluble extract transformed with pET28a6HIS-Δ38NADKc (40 µg); lane 3: Ni-NTA pool (10 µg); lane 4: urea-denatured 6HIS-Δ38NADKc purified on Ni-NTA (10 µg); lane 5: refolded 6HIS-Δ38NADKc (2 µg).

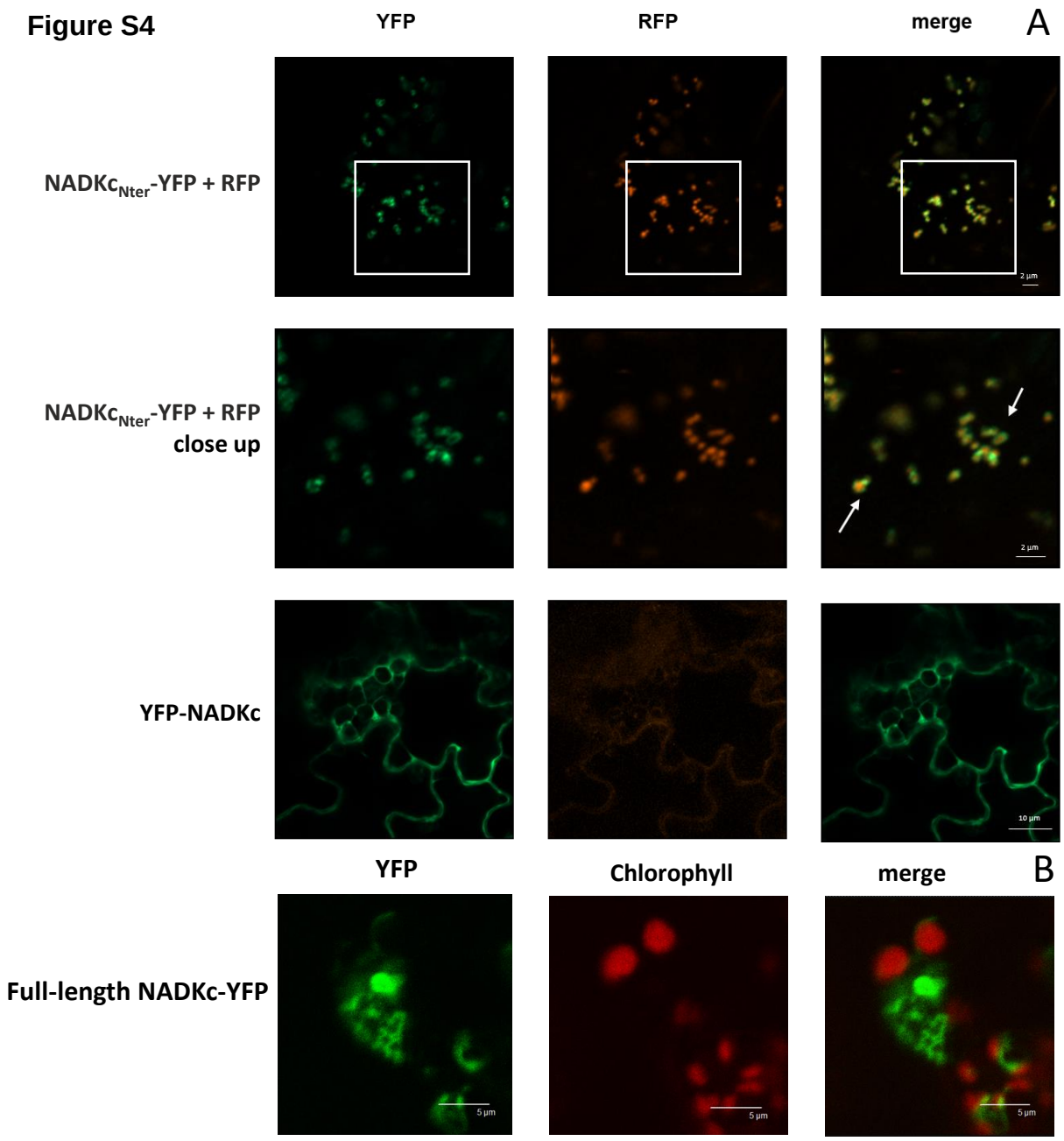

Supplemental Figure S4. A. NADKc$_{Nter}$-YFP associates with mitochondria in *N. benthamiana* leaves. Representative pictures of transiently transformed *N. benthamiana* leaf cells. Left: YFP (green), Center: RFP (red), and Right: merged fluorescence. The top row shows a representative image of *N. benthamiana* cells co-transformed with the NADKc$_{Nter}$-YFP construct and a mitochondrial marker, pSu9–RFP. The second row shows a close-up of mitochondria from the lower right region of the images in the top row (white boxes). White arrows indicate regions in which the YFP signal appears peripheral with respect to the RFP signal. The third row shows a representative image of *N. benthamiana* cells transformed with the YFP-NADKc construct alone. The central image shows the background signal in the RFP channel. White bars represent 2 µm in the first and second row, and 10 µm in the third row. **B**. Full length NADKc-YFP stably expressed in Arabidopsis forms aggregates in the cytosol. White bars represent 5 µm.

Figure S5

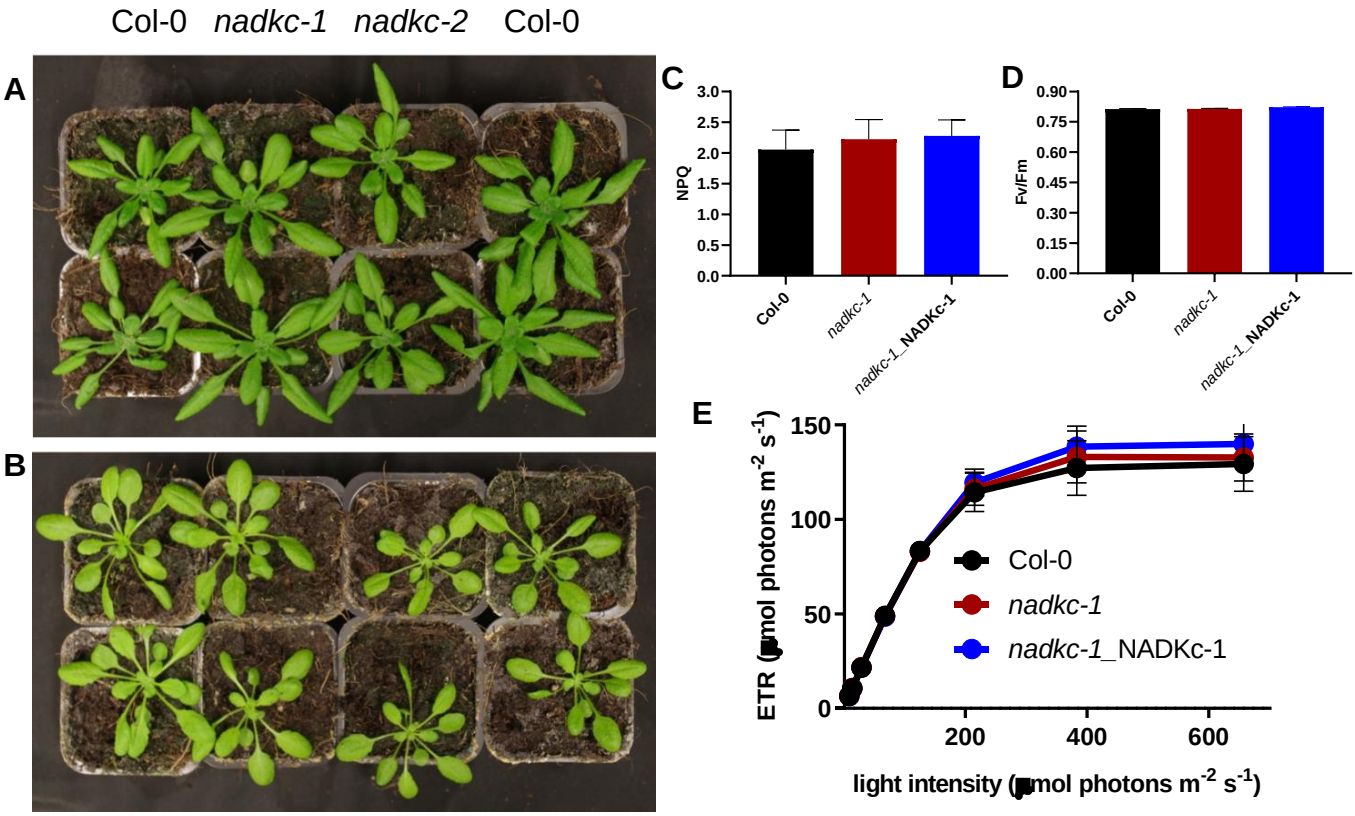

Supplemental Figure S5. Phenotype of *nadkc* mutants. (A) 21-day-old plants grown under long day photoperiod (16 h light/8 h dark); (B) 28-day-old plants grown under short day photoperiod (8 h light/16 h dark). (C-E) Photosynthetic parameters in Col-0 and *nadkc* plants: (C) NPQ, (D) Fv/Fm and (E) electron transport rate.

Figure S6

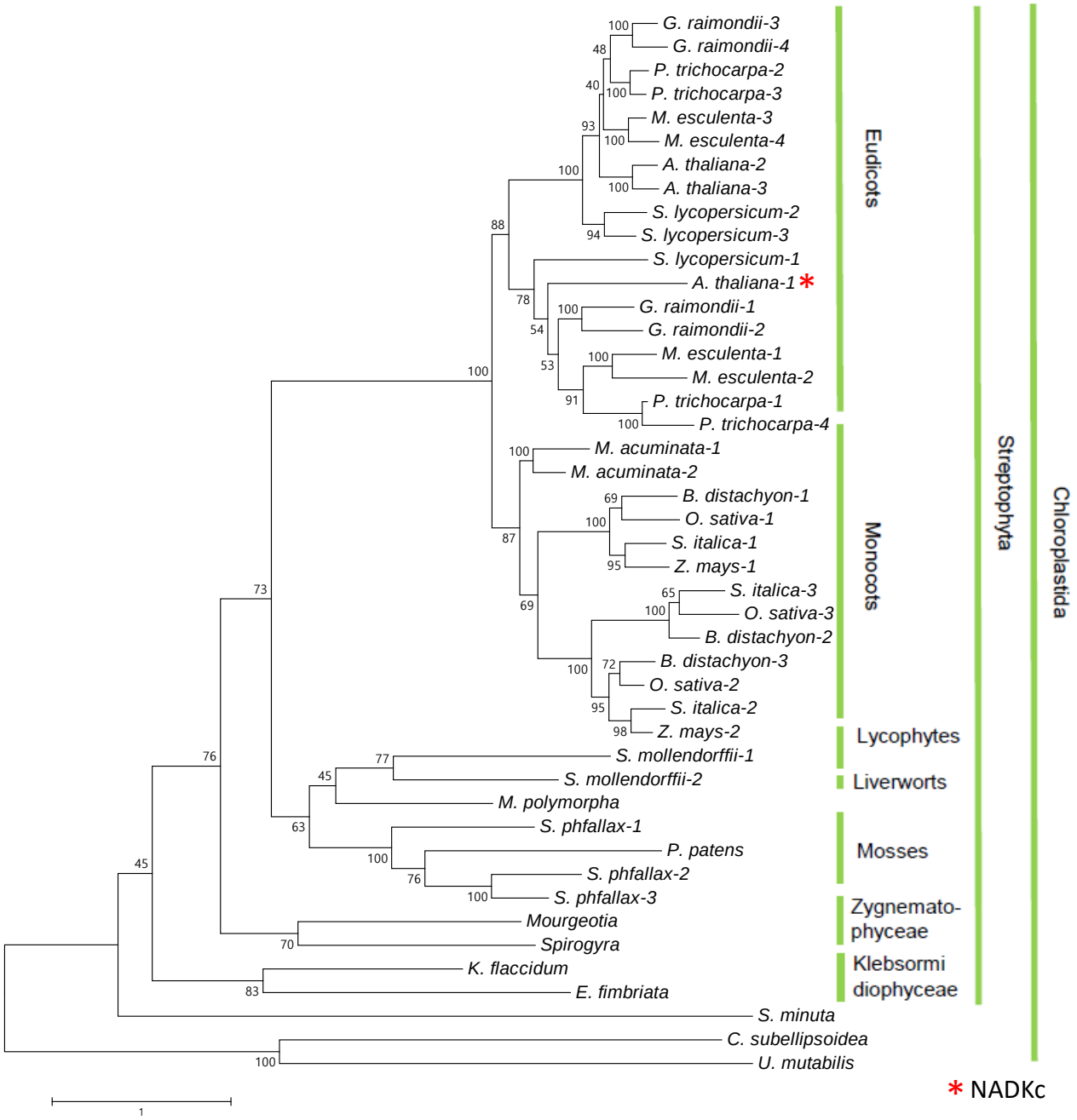
G. raimondii-3
G. raimondii-4
P. trichocarpa-2
P. trichocarpa-3
M. esculenta-3
M. esculenta-4
A. thaliana-2
A. thaliana-3
S. lycopersicum-2
S. lycopersicum-3
S. lycopersicum-1
A. thaliana-1 *
G. raimondii-1
G. raimondii-2
M. esculenta-1
M. esculenta-2
P. trichocarpa-1
P. trichocarpa-4
M. acuminata-1
M. acuminata-2
B. distachyon-1
O. sativa-1
S. italica-1
Z. mays-1
S. italica-3
O. sativa-3
B. distachyon-2
B. distachyon-3
O. sativa-2
S. italica-2
Z. mays-2
S. mollendorffii-1
S. mollendorffii-2
M. polymorpha
S. phfallax-1
P. patens
S. phfallax-2
S. phfallax-3
Mourgeotia
Spirogyra
K. flaccidum
E. fimbriata
S. minuta
C. subellipsoidea
U. mutabilis
Eudicots
Monocots
Lycophytes
Liverworts
Mosses
Zygnemato-phyceae
Klebsormi diophyceae
Streptophyta
Chloroplastida
* NADKc

Supplementary Fig. S6. Phylogeny of NADKc. Maximum likelihood phylogenetic tree of NADKc-like proteins in the following plant and algal species: *Arabidopsis thaliana* (*A. thaliana*), *Populus trichocarpa* (*P. trichocarpa*), *Manihot esculenta* (*M. esculenta*), *Gossypium raimondii* (*G. raimondii*), *Solanum lycopersicum* (*S. lycopersicum*), *Setaria italica* (*S. italica*), *Zea mays* (*Z. mays*), *Oryza sativa* (*O. sativa*), *Brachypodium distachyon* (*B. distachyon*), *Musa acuminata* (*M. acuminata*), *Marchantia polymorpha* (*M. polymorpha*), *Physcomitrella patens* (*P. patens*), *Sphagnum phallax* (*S. phallax*), *Selaginella mollendorffii* (*S. mollendorffii*) *Klebsormidium flaccidum* (*K. flaccidium*), *Coccomyxa subellipsoidea* (*C. subellipsoidea*), *Ulva mutabilis* (*U. mutabilis*), *Spirotaenia minuta* (*S. minuta*), Mougeotia sp., Spirogyra sp. and *Entransia fimbriata* (*E. fimbriata*). Accession numbers: *A. thaliana-1* (NADKc): At1g04280, *A. thaliana-2*: At1g06750, *A. thaliana-3*: At2g30630, *P. trichocarpa-1*: Potri.008G162000, *P. trichocarpa-2*: Potri.002G043000, *P. trichocarpa-3*: Potri.005G220000, *P. trichocarpa-4*: Potri.008G162400, *M. esculenta-1*: Manes.15G036900, *M. esculenta-2*: Manes.03G168900, *M. esculenta-3*: Manes.01G200600, *M. esculenta-4*: Manes.05G086200, *G. raimondii-1*: Gorai.011G171100, *G. raimondii-2*: Gorai.006G246600, *G. raimondii-3*: Gorai.004G074100, *G. raimondii-4*: Gorai.013G104300, *S. lycopersicum-1*: Solyc06g053810, *S. lycopersicum-2*: Solyc06g031670, *S. lycopersicum-3*: Solyc08g059750, *S. italica-1*: Seita.9G163700, *S. italica-2*: Seita.3G185100, *S. italica-3*: Seita.5G337000, *Z. mays-1*: GRMZM2G070252, *Z. mays-2*: GRMZM2G368410, *O. sativa-1*: Os03g43010, *O. sativa-2*: Os05g43300, *O. sativa-3*: Os01g56764, *B. distachyon-1*: Bradi1g14307, *B. distachyon-2*: Bradi2g51490, *B. distachyon-3*: Bradi2g20400, *M. acuminata-1*: SMUA_Achr5T03210, *M. acuminata-2*: GSMUA_Achr7T01560, *M. polymorpha*: Mapoly0142s0012, *P. patens*: Pp3c2_3490V3, *S. phallax-1*: Sphallax0059s0037, *S. phallax-2*: Sphallax0011s0002, *S. phallax-3*: Sphallax0120s0019, *S. mollendorffii-1*: scaffold 73427, *S. mollendorfii-2*: scaffold 231175, *K. flaccidum*: kfl00274_0130, *C. subellipsoidea*: XP_005648203, *U. mutabilis*: UM028_0076.1, *S. minuta*: NNHQ_2000691, *Mougeotia*: ZRMT_2002068, *Spirogyra*: HAOX_2025158, *E. fimbriata*: BFIK_2025349. The tree is drawn to scale, with branch lengths measured in the number of substitutions per site (scale bar in the bottom-left corner). The numbers at the interior nodes are bootstrap percentages.

Supplemental Table S1

Pep	Number of identified peptides
SC	Spectral Counts: mass spectra allow the identification of peptides belonging to the protein
SSC	Specific Spectral Counts: mass spectra allow the identification of peptides belonging specifically to the protein
	Identified only in Eluate sample with SSC ≥ 5 or enriched at least 10 times in Eluate sample compared to Flowthrough sample
	At1g04280 (NADK4)

Accession	Protein name	Coverage	Mol. Weight (blue: less than 50 kDa; red: higher than 65 kDa; green: between 50 and 65 kDa)	SSC Eluate / SSC Flowthrough	Flowthrough			Eluate			putative ATP binding domain (aa) - Interpro (nd: not detected)	putative CaM-binding domain (nd: not detected)	Comments
					Pep	SC	SSC	Pep	SC	SSC			
RNJ_ARATH	Ribonuclease J	33.37	100554	Eluate only				29	34	34	nd	210-224	
RH42_ARATH	RNA helicase 42	20.24	133033	Eluate only				25	28	28	560-738	866-880; 990-1001	
ICR1_ARATH	Interactor of constitutive active ROPs 1	52.03	38358	Eluate only				19	22	22	nd	258-276	
PARNL_ARATH	Poly(A)-specific ribonuclease PARN-like	24.43	68807	Eluate only				16	18	18	nd	190-207; 223-238	
A0A178W9E9_ARATH	Obg-like ATPase 1	28.27	45628	Eluate only				10	17	17	54-359	31-46	
MED16_ARATH	Mediator of RNA polymerase II transcription subunit 16	15.81	138187	Eluate only				15	17	17	nd	1211-1224	
Q9SYM7_ARATH	2-oxoglutarate (2OG) and Fe(II)-dependent oxygenase superfamily protein	26.97	41015	Eluate only				10	14	14	nd	175-193	
TON1A_ARATH	Protein TONNEAU 1a	37.31	29334	Eluate only				13	14	13	nd	15-30	
ODP23_ARATH	Dihydrolipoyllysine-residue acetyltransferase component 3 of pyruvate dehydrogenase complex, mitochondrial	23.19	58467	Eluate only				11	14	13	nd	13-22; 354-367	
PHOT2_ARATH	Phototropin-2	15.08	102472	Eluate only				15	15	13	583-606	852-868	
STA1_ARATH	Protein STABILIZED1	11.66	115576	Eluate only				12	13	13	nd	749-765; 842-857; 930-945	
UGPA2_ARATH	UTP--glucose-1-phosphate uridylyltransferase 2	25.59	51738	Eluate only				10	13	13	nd	249-277; 397-415	
ATPG1_ARATH	ATP synthase gamma chain 1, chloroplastic	31.37	40911	Eluate only				10	12	12	nd	75-83; 140-159	
EBFC2_ARATH	Nucleoid-associated protein At2g24020, chloroplastic	44.51	19812	Eluate only				13	15	12	nd	36-55; 79-98; 140-159	
PR35B_ARATH	Pre-mRNA-processing protein 40B	15.93	113569	Eluate only				11	12	12	nd	489-503	
PSD3_ARATH	Phosphatidylserine decarboxylase proenzyme 3	17.32	70352	Eluate only				10	12	12	nd	455-462	
SUOX_ARATH	Sulfite oxidase	34.1	43329	Eluate only				10	12	12	nd	101-117	
DOT2_ARATH	SART-1 family protein DOT2	17.32	94142	Eluate only				10	11	11	nd	618-637; 643-662	
COIL_ARATH	Coilin	12.5	68667	Eluate only				9	11	11	nd	15-26	
NEDD1_ARATH	Protein NEDD1	20.97	84757	Eluate only				9	11	11	nd	110-122	
PTA16_ARATH	Protein PLASTID TRANSCRIPTIONALLY ACTIVE 16, chloroplastic	26.47	54358	Eluate only				9	10	10	nd	25-32	
A0A178V7A8_ARATH	Uncharacterized protein AXX17_At4g18270	27.95	43910	Eluate only				8	10	10	nd	240-254	
E135_ARATH	Glucan endo-1,3-beta-glucosidase 5	21.28	52715	Eluate only				8	10	10	nd	51-59	
SH3P3_ARATH	SH3 domain-containing protein 3	28.77	39534	Eluate only				8	10	10	nd	230-247	
TON1B_ARATH	Protein TONNEAU 1b	30.74	29185	Eluate only				10	10	9	nd	15-30	
PDPK1_ARATH	3-phosphoinositide-dependent protein kinase 1	18.74	54711	Eluate only				8	9	9	30-339	58-75	Protein kinase
A0A178USK6_ARATH	Uncharacterized protein AXX17_At4g37900	23.19	56571	Eluate only				9	9	8	94-402	105-118	Protein kinase
Q0WUY1_ARATH	p-loop containing nucleoside triphosphate hydrolases superfamily protein (At1g04280)	15.33	60166	Eluate only				8	8	8	224-365	181-188	
A0A1P8BE11_ARATH	RabGAP/TBC domain-containing protein	19.15	78317	Eluate only				7	8	8	nd	68-81	
AT13A_ARATH	Autophagy-related protein 13a	11.44	66564	Eluate only				6	8	8	nd	140-147	
C3H38_ARATH	Zinc finger CCCH domain-containing protein 38	11.24	75581	Eluate only				7	8	8	nd	620-636	
NFXL1_ARATH	NF-X1-type zinc finger protein NFXL1	8.92	130716	Eluate only				8	8	8	nd	936-951	
PP1R8_ARATH	Protein phosphatase 1 regulatory inhibitor subunit PPP1R8 homolog	16.26	39985	Eluate only				5	8	8	nd	153-168; 224-238	
PUX9_ARATH	Plant UBX domain-containing protein 9	23.24	52136	Eluate only				7	8	8	nd	412-431	
TPLAT_ARATH	Protein TPLATE	11.39	130908	Eluate only				8	8	8	nd	217-233	
A0A178UB82_ARATH	Fe2OG dioxygenase domain-containing protein	16.95	39678	Eluate only				7	7	7	nd	321-337	
A0A178V0X9_ARATH	SAP domain-containing protein	13.86	69578	Eluate only				7	7	7	nd	nd	
A0A178V6Z0_ARATH	Uncharacterized protein AXX17_At4g35270	12.79	65126	Eluate only				6	7	7	nd	140-159	
A0A178VQ14_ARATH	PIA1	25.81	30497	Eluate only				6	7	7	nd	31-48	
A0A178W283_ARATH	WD_REPEATS_REGION domain-containing protein	12.94	71331	Eluate only				5	7	7	nd	448-466	
A0A178WAH4_ARATH	SurE domain-containing protein	26.75	40674	Eluate only				7	7	7	nd	293-307	
BIM2_ARATH	Transcription factor BIM2	32.15	34487	Eluate only				7	7	7	nd	254-271	
DNLI1_ARATH	DNA ligase 1	11.14	87740	Eluate only				7	7	7	nd	137-154; 516-533	
F4K465_ARATH	Nucleoporin-like protein	12.86	81685	Eluate only				7	7	7	nd	22-38	
GEML1_ARATH	GEM-like protein 1	26.64	27958	Eluate only				6	7	7	nd	124-142	
PTN2B_ARATH	Phosphatidylinositol 3,4,5-trisphosphate 3-phosphatase and protein-tyrosine-phosphatase PTEN2B	19.94	70073	Eluate only				7	7	7	nd	171-181	
TAF4B_ARATH	Transcription initiation factor TFIID subunit 4b	11.03	93741	Eluate only				6	7	7	nd	208-222	
TYW23_ARATH	tRNA wybutosine-synthesizing protein 2/3/4	6.23	110856	Eluate only				5	7	7	nd	687-700	
A0A178UKW5_ARATH	2-(3-amino-3-carboxypropyl)histidine synthase subunit 1	16.78	50341	Eluate only				6	6	6	70-374	277-289	Monosaccharide transporter 3 (Schneidereit et al, 2003)
A0A178UGE6_ARATH	Uncharacterized protein AXX17_At5g58590	20.97	48903	Eluate only				6	6	6	nd	6-25	
A0A178UX40_ARATH	SWIB domain-containing protein	33.33	15999	Eluate only				8	12	6	61-144	nd	
A0A178W3D1_ARATH	Uncharacterized protein AXX17_At1g75860	29.11	24258	Eluate only				4	6	6	nd	123-136	
A0A178WJI9_ARATH	J domain-containing protein	19.93	31907	Eluate only				6	6	6	nd	215-232	
A0A178WC39_ARATH	Uncharacterized protein AXX17_At1g53280	9.87	86016	Eluate only				6	6	6	nd	126-144	
A0A178WE72_ARATH	GYF domain-containing protein	4.15	166231	Eluate only				5	6	6	nd	nd	
DUF7_ARATH	DUF724 domain-containing protein 7	9.97	80740	Eluate only				6	6	6	nd	41-49	
PATL3_ARATH	Patellin-3	10.61	56105	Eluate only				4	6	6	nd	174-187; 259-267	
PDI21_ARATH	Protein disulfide-isomerase like 2-1	18.84	39497	Eluate only				6	6	6	nd	302-316	
SLU7A_ARATH	Pre-mRNA-splicing factor SLU7-A	10.47	61978	Eluate only				5	6	6	nd	82-96	
SUR1_ARATH	S-alkyl-thiohydroximate lyase SUR1	17.97	51088	Eluate only				6	6	6	nd	37-50	
ICR4_ARATH	Interactor of constitutive active ROPs 4	24.38	36057	Eluate only				4	5	5	nd	nd	
A0A178VKF6_ARATH	RRM domain-containing protein	6.65	73124	Eluate only				4	5	5	nd	520-534	
A0A178W2B9_ARATH	Uncharacterized protein AXX17_At1g09880	14.78	54855	Eluate only				5	5	5	nd	234-249	
AT18H_ARATH	Autophagy-related protein 18h	5.72	100514	Eluate only				5	5	5	nd	307-323	
BLI_ARATH	Protein BLISTER	7.00	78384	Eluate only				5	5	5	nd	629-648	
CBSX2_ARATH	CBS domain-containing protein CBSX2, chloroplastic	16.81	25956	Eluate only				3	5	5	83-145; 177-234	157-174; 216-233	
DEG15_ARATH	Glyoxysomal processing protease, glyoxysomal	6.63	76126	Eluate only				4	5	5	nd	539-555	
HIS4_ARATH	Imidazole glycerol phosphate synthase hisHF, chloroplastic	11.66	64192	Eluate only				5	5	5	nd	276-283	
Q8GUK8_ARATH	At5g10060	13.86	51955	Eluate only				5	5	5	nd	105-121	
TBA2_ARATH	Tubulin alpha-2 chain	14.67	49541	Eluate only				4	5	5	nd	154-167	
A0A1P8BFF0_ARATH	Acyl-CoA binding protein 5	34.58	73292	Eluate only	7	9	0	22	38	17	nd	304-320	
HS901_ARATH	Heat shock protein 90-1	17.86	80635	Eluate only	2	3	0	13	14	10	27-181	323-348	Protein kinase
AROD3_ARATH	Arogenate dehydratase 3, chloroplastic	26.42	46102	Eluate only	1	1	0	8	9	8	nd	319-330	
PATL1_ARATH	Patellin-1	18.32	64046	Eluate only	2	2	0	9	12	8	nd	264-278	
A1L4Y1_ARATH	At3g10350	37.71	44754	38,00	1	1	1	18	38	38	nd	263-282	
NIR_ARATH	Ferredoxin--nitrite reductase, chloroplastic	42.32	65505	34,00	1	1	1	26	34	34	nd	311-328	
DCE2_ARATH	Glutamate decarboxylase 2	42.11	56141	20,50	4	5	2	36	63	41	nd	465-490	
SECA1_ARATH	Protein translocase subunit SECA1, chloroplastic	16.24	115183	20,00	1	1	1	19	20	20	92-302; 423-470; 471-580; 677-760	489-502	
PR40C_ARATH	Pre-mRNA-processing protein 40C	16.17	92807	17,00	1	1	1	14	17	17	nd	687-705	
A0A178UKA9_ARATH	Uncharacterized protein AXX17_At5g10570	36.87	48691	15,00	1	1	1	14	15	15	nd	259-268	
F4K0R0_ARATH	Transducin family protein / WD-40 repeat family protein	17.11	120063	14,00	1	1	1	14	14	14	nd	609-624	
CRWN1_ARATH	Protein CROWDED NUCLEI 1	31.1	129093	13,25	4	4	4	44	53	53	nd	953-971	
A0A178UHM4_ARATH	Uncharacterized protein AXX17_At5g00220	24.63	52331	13,00	1	1	1	12	13	13	nd	124-141	
A0A178URW9_ARATH	At5g30145	33.9	26061	12,00	1	1	1	8	12	12	nd	157-176	
A0A178U844_ARATH	Signal recognition particle subunit SRP68	31.24	68833	11,50	2	2	2	20	23	23	nd	66-84; 353-367	
ALFC5_ARATH	Fructose-bisphosphate aldolase 5, cytosolic	25.7	38294	11,00	2	2	1	9	12	11	nd	131-145; 305-316	
CAP2_ARATH	Putative clathrin assembly protein At2g25430	13.02	72084	10,00	1	1	1	9	10	10	nd	65-81	
DCE4_ARATH	Glutamate decarboxylase 4	38.74	56005	10,00	6	7	1	27	49	10	nd	356-370	
Q9SK61_ARATH	Expressed protein At2g20410	32.74	37569	10,00	1	1	1	9	10	10	nd	17-34	

Table S2: Primers used in this study

In red: sequences for recombination reactions by BP clonase into pDONR221.

Uppercase: restriction enzyme sites.

Primers for cloning the NADKc protein sequence for enzymatic, localization and complementation studies:

construct	Forward primer	Reverse primer
pet28(b)-6-HIS-NADKc	gacttttcaaaccaaCATATGgtgaaaccttaggagaag	caaattcaggaagaagaCTCGAGcaaaggtctagttc
pet28(b)-6-HIS-D38NADKc	gctgtagcagctCATATGgccggagaattactc	caaattcaggaagaagaCTCGAGcaaaggtctagttc
35S::NADKc$_{Nter}$-YFP (in pB7YWG2,0)	GGGGACAAGTTTGTACAAAAAAGCAGGCTTgatggtgaaacccttaggagaag	GGGGACCACTTTGTACAAGAAAGCTGGGTggacatctttataccccatg
35S::NADKc-YFP (in pB7YWG2,0)	GGGGACAAGTTTGTACAAAAAAGCAGGCTTgatggtgaaacccttaggagaag	GGGGACCACTTTGTACAAGAAAGCTGGGTatttttttggttgggccttttcgattctcc
35S::YFP-NADKc (in pB7WGY2,0) and 35S::NADKc (in pB2GW7,0)	GGGGACAAGTTTGTACAAAAAAGCAGGCTTgatggtgaaacccttaggagaag	GGGGACCACTTTGTACAAGAAAGCTGGGTtcaatttttttggttgggccttttcgattcctcc

Primers for genotyping:

line	Forward primer	Reverse primer	LB primer
SALK_130871	tgttaagcaaatatgtggggcc	acaaatgatcgaaatggcaag	LBb1.3 attttgccgattttcggaac
GABI_311H11	taaggaagaaggacgggacttc	tcaagatcgaccaaagcattag	LBgabi-kat atattgaccatcatactcattgc

Primers for gene expression studies (qPCR):

	Forward primer	Reverse primer
At1g04280	aacgggtcagcagtctcaac	gggcctcgatggaactaaca